Measuring electron gyro-scale fluctuations in NSTX plasmas using a collective scattering system

David R. Smith
Princeton Plasma Physics Lab

In collaboration with:

E. Mazzucato and H.K. Park
Princeton Plasma Physics Lab
W. Lee
Pohang University
C.W. Domier and N.C. Luhmann, Jr.
University of California at Davis

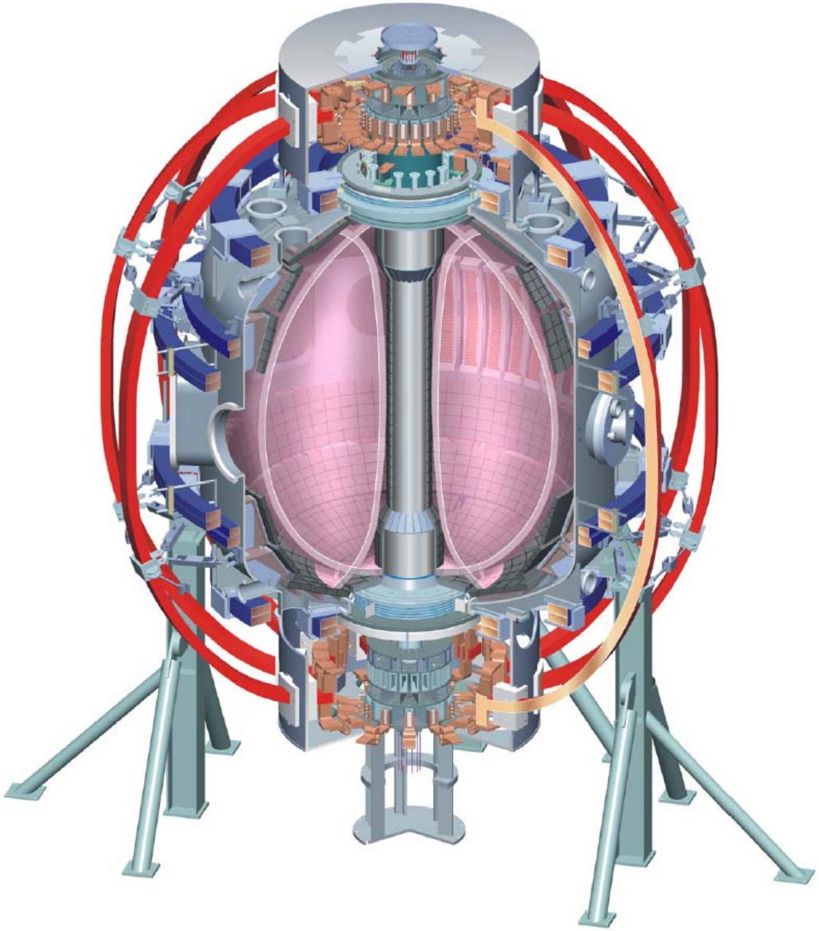

Plasma Science & Technology Dept. Seminar
Princeton Plasma Physics Lab
December 7, 2007

Outline

- Motivation
  - Does electron temperature gradient (ETG) turbulence produce meaningful electron thermal transport?
- Principles of scattering measurements
- The NSTX high-k scattering system
  - Core fluctuation diagnostic with high sensitivity, spatial localization, k-space selectivity for up to five distinct wavenumbers, and steerable optics.
- Initial measurements and research topics

ETG turbulence and electron thermal transport

Transport sets the plasma size needed to attain fusion-relevant conditions

NSTX

The perpendicular particle flux ($\Gamma_\perp$) and perpendicular energy flux ($Q_\perp$) are key transport quantities

0th moment: $$\frac{\partial n}{\partial t} + \boxed{\nabla \cdot (n\vec{V})} = S_p \overset{\int dV}{\Rightarrow} \frac{\partial N}{\partial t} + \boxed{\vec{\Gamma} \cdot \hat{r}} = S_p V$$

1st moment (SS): $$\boxed{\vec{\Gamma}_\perp \equiv n\vec{V}_\perp = \frac{1}{qB}\hat{b} \times \left[\nabla \cdot \overleftrightarrow{P} - qn\vec{E} - \vec{S}_m\right]}$$

2nd moment: $$\frac{\partial}{\partial t}\left(\frac{3}{2}p + \frac{1}{2}mnV^2\right) + \boxed{\nabla \cdot \vec{Q}} = qn\vec{E} \cdot \vec{V} + S_e \overset{\int dV}{\Rightarrow} \frac{\partial E}{\partial t} + \boxed{\vec{Q} \cdot \hat{r}} = H_{tot} V$$

3rd moment (SS): $$\boxed{\vec{Q}_\perp = \frac{1}{\Omega}\hat{b} \times \left[\nabla \cdot \overleftrightarrow{R} - \frac{5}{2}\frac{q}{m}p\vec{E} - \frac{q}{m}\overleftrightarrow{\pi} \cdot \vec{E} - qn\vec{E} \cdot \left(\frac{1}{2}V^2\overleftrightarrow{I} + \vec{V}\vec{V}\right) - \vec{S}_{ef}\right]}$$

terms with substantial fluctuation contributions

(species subscripts suppressed above)

Fluctuation-induced transport typically dominates other contributions

Fluctuation-induced particle and energy transport

$$\vec{\Gamma}_{\perp}^{fl} = \left\langle \tilde{n}\tilde{\vec{v}}_E \right\rangle \qquad \vec{Q}_{\perp}^{fl} = \frac{5}{2}\left\langle \tilde{p}\tilde{\vec{v}}_E \right\rangle$$

The phase between fluctuations is critical.

When $\tilde{n}$ leads $\tilde{\phi}$ (non-adiabatic response), there is a net motion of particles down the density gradient.

The story is the same for energy and $\tilde{p}$.

What drives electron thermal transport?

NSTX

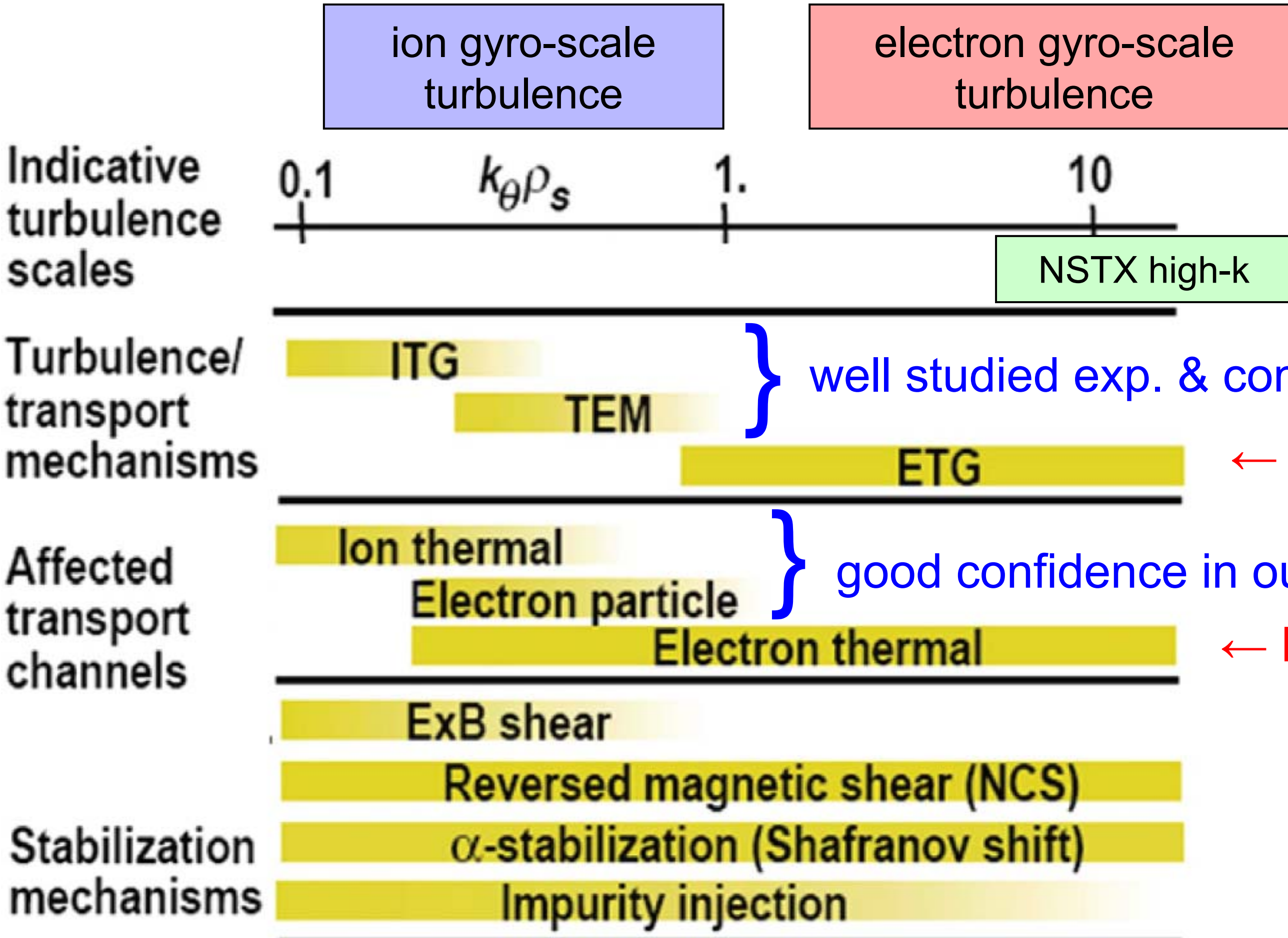

} well studied exp. & comp.

← long disregarded until recently

} good confidence in our understanding

← low confidence

[Doyle et al., NF 47, S18 (2007)]

note that fusion α particles will preferentially heat electrons

Electron thermal transport is typically the dominant loss channel in NSTX plasmas

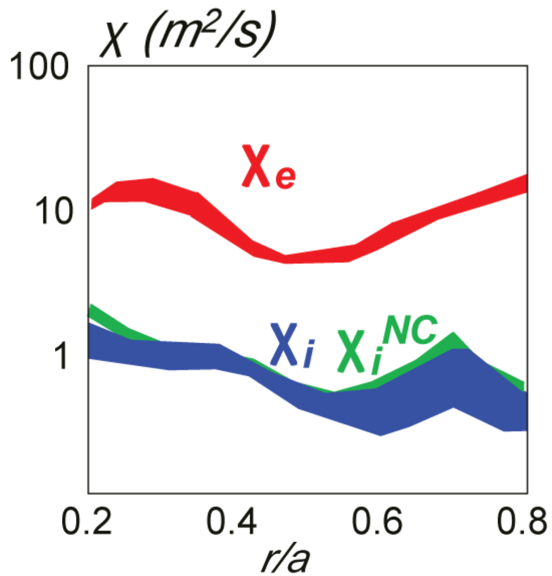

Stutman, APS 04

Ion thermal transport is at or near neoclassical.

It is widely held that ExB flow shear stabilizes ITG/TEM turbulence in NSTX.

[see papers by Kaye (07, 06), Levinton (07), Stutman (06), LeBlanc (04), Synakowski (03), Bourdelle (03), Rewolt (96)]

Relation between energy flux Q_s and heat flux q_s:

$$\vec{Q}_s = \vec{q}_s + \frac{5}{2} p_s \vec{V}_s + O(\delta^2)$$

Common thermal transport model:

$$\vec{q}_s = \chi_s \nabla T_s$$

thermal conductivity

Drift-interchange modes are analogous to the Rayleigh-Taylor instability

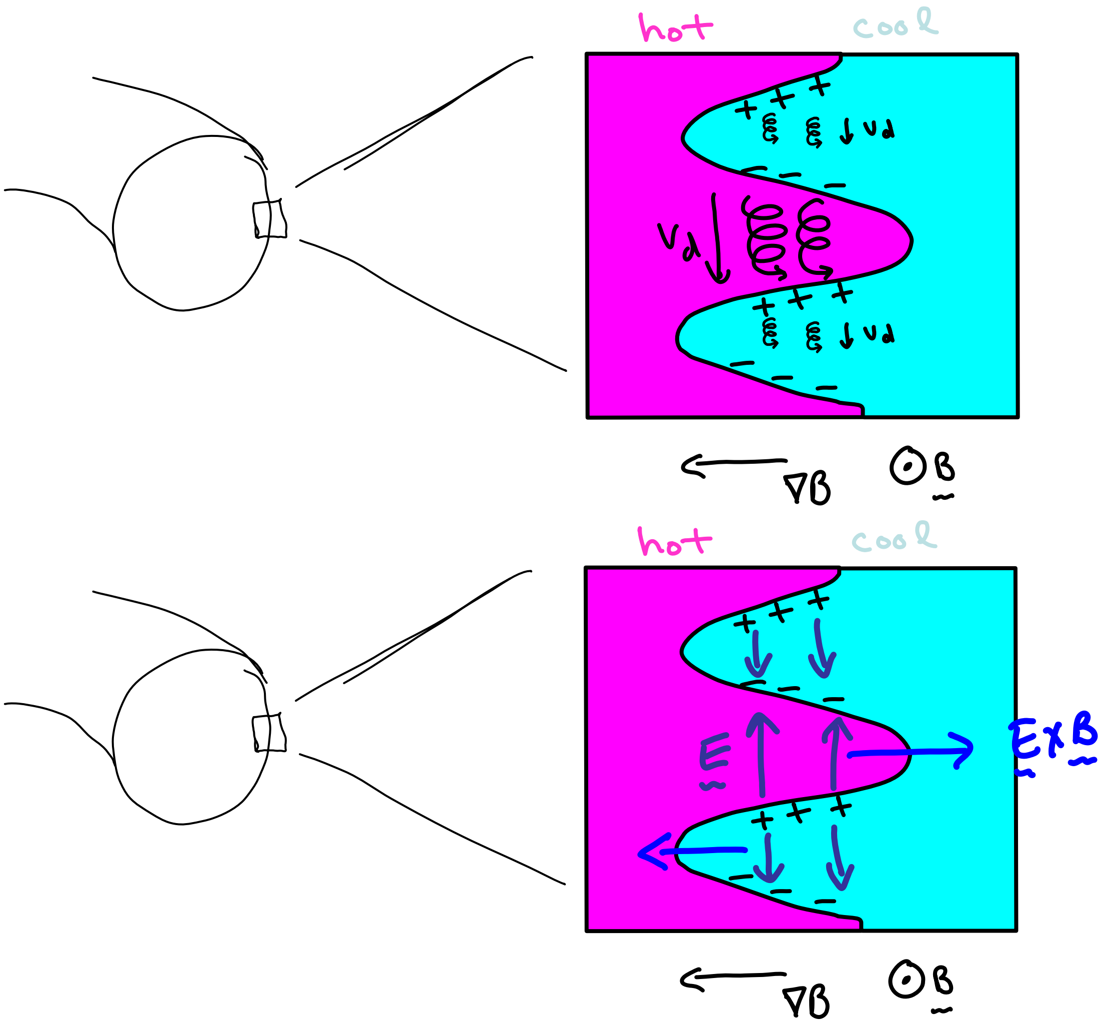

"Gravity" is ExB drift arising from charge separation due to ∇B/curvature drifts

Generic drift-interchange growth rate:

$$\gamma = \frac{v_t}{\sqrt{RL_p}}$$

[G. Hammett, APS 2007 Review Talk]

Plasma turbulence is anisotropic with $k_\perp \gg k_{||}$

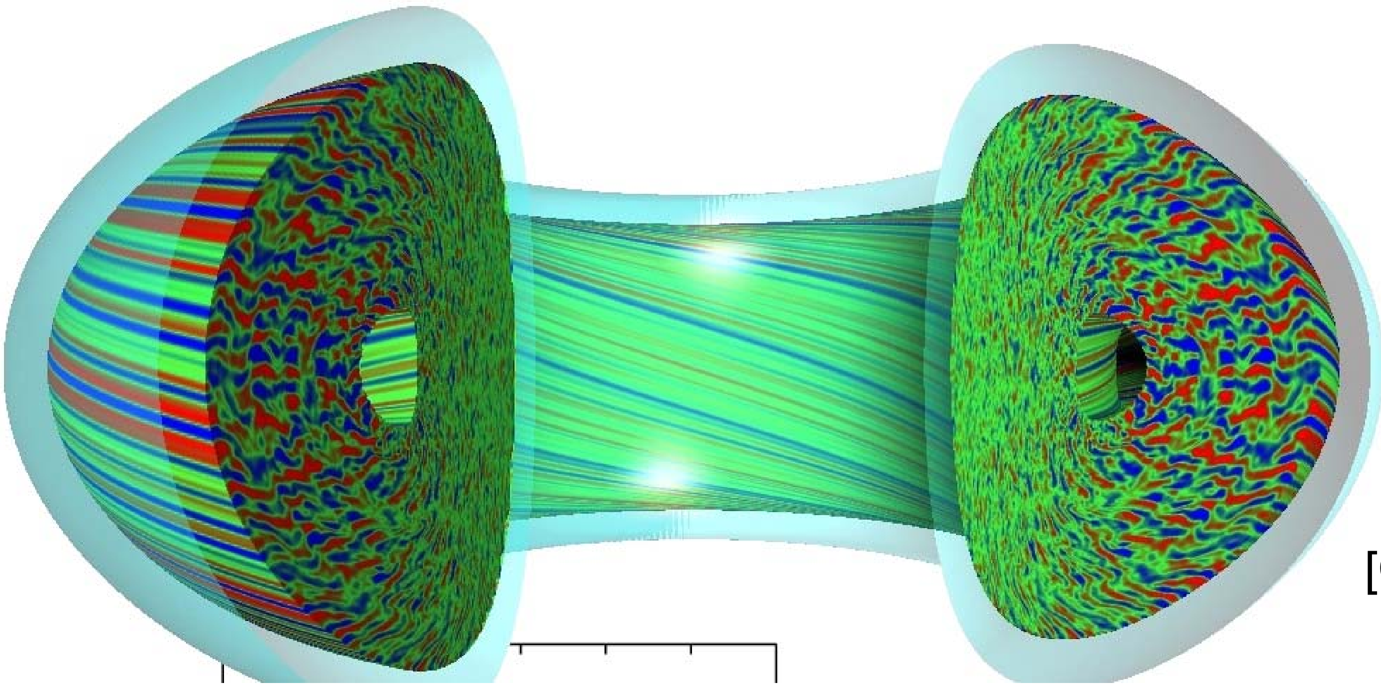

[Candy, Waltz, and the GYRO team]

$$k_\perp \rho_x \sim O(1) \quad \text{and} \quad k_{||} qR \sim O(1) \quad \Rightarrow$$

$$kB >> \vec{k} \cdot \vec{B} \approx 0 \quad \text{and} \quad \boxed{k_\perp >> k_{||}}$$

Remember this for later...

ETG instability exhibits a critical gradient

ETG critical gradient from linear gyrokinetic simulations using GS2 [Jenko, PoP 8, 4096 (2001)]

$$\left(\frac{R}{L_{Te}}\right)_{crit} = \mathrm{Max}\left\{\left(1+\frac{Z_{eff}T_e}{T_i}\right)\left(1.33+1.91\frac{\hat{s}}{q}\right)(1-1.5\varepsilon)\left(1+0.3\varepsilon\frac{d\kappa}{d\varepsilon}\right),\ 0.8\frac{R}{L_{ne}}\right\}$$

ETG critical gradient extends to nonlinear saturation and electron thermal transport

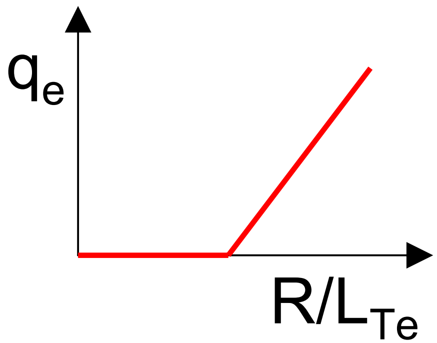

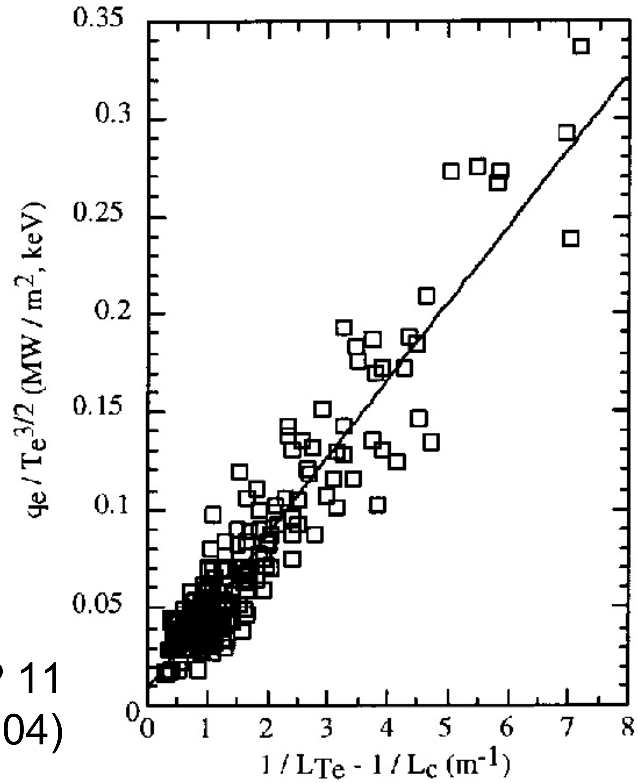

Horton, PoP 11 2600 (2004)

ETG turbulence can saturate at higher amplitude than ITG/TEM turbulence due to zonal flow dynamics

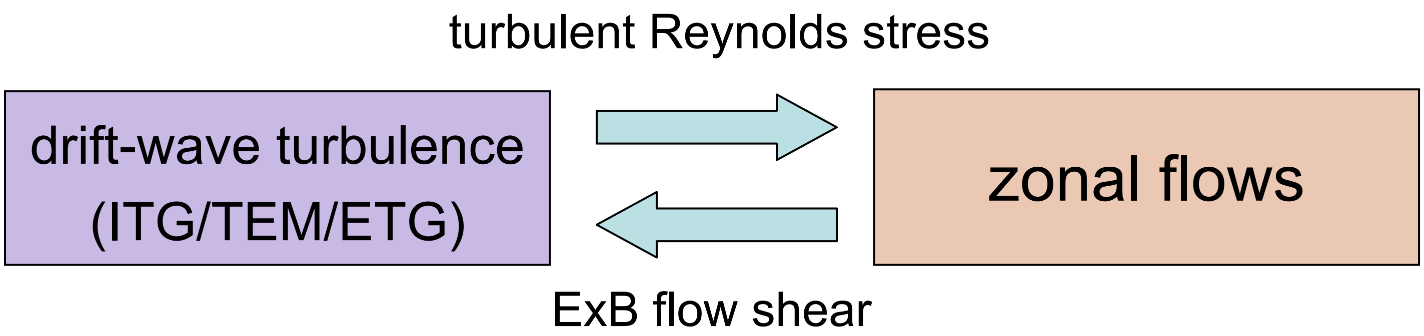

ETG turbulence generates zonal flows less efficiently than ITG/TEM turbulence because the adiabatic-ions in ETG turbulence have large gyro-orbits compared to ETG-driven zonal flows.

Consequently, ETG turbulence saturates at higher amplitude and produces more normalized transport than ITG/TEM turbulence.
[see Dorland, PRL (2000) and Nevins, PoP (2006)]

$$\frac{\chi_e^{ETG}}{\chi_e^{gB}} \sim 2-5 \qquad \frac{\chi_i^{ITG}}{\chi_i^{gB}} \sim 0.5-2$$

Scattering measurements of plasma turbulence

Layout of a scattering system

- The intersection of the probe beam and receiving beam defines the scattering volume
- The scattering angle provides k-space selectivity through the Bragg relation: $k = 2k_i \sin(\theta/2)$

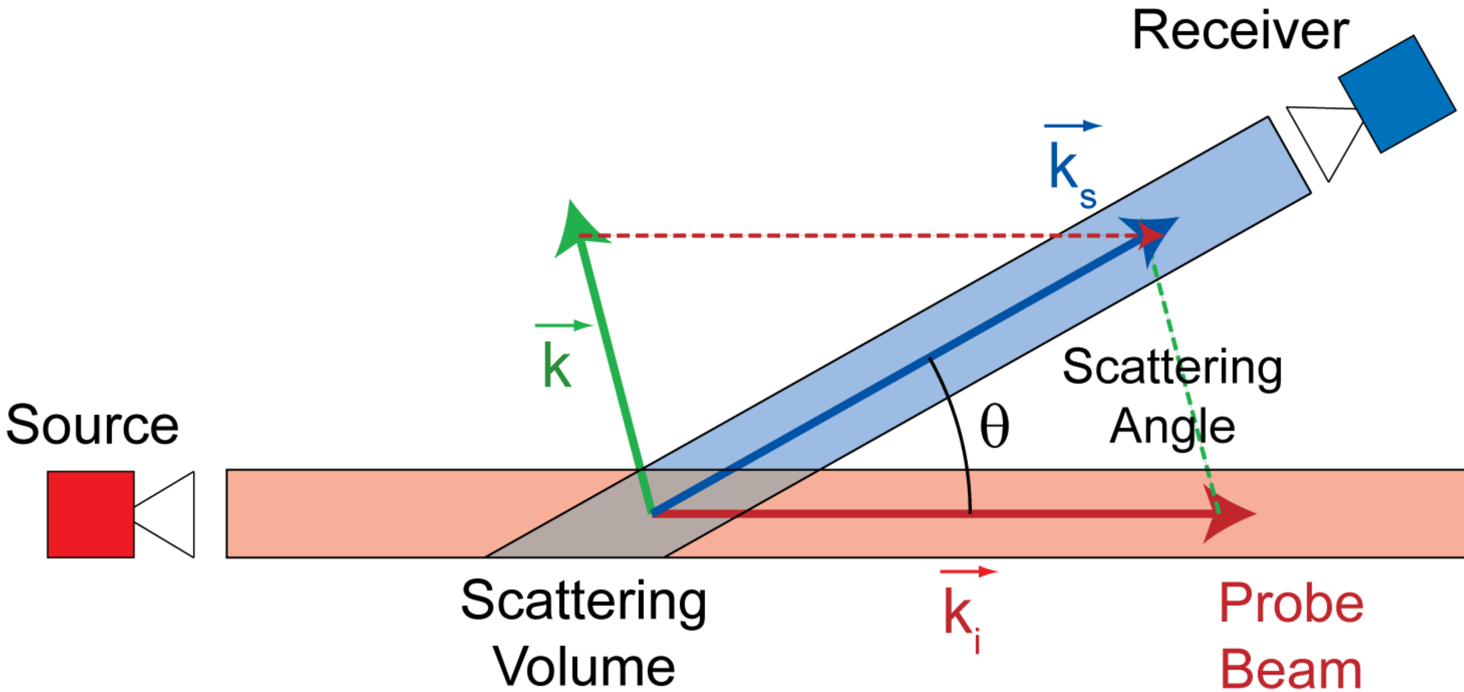

Conservation relations describe three-wave coupling among EM waves and a plasma fluctuation

An incident EM wave (k_i, ω_i) and a plasma fluctuation (k, ω) couple to produce a scattered EM wave (k_s, ω_s).

Momentum conservation:

$$\vec{k}_s = \vec{k}_i \pm \vec{k}$$

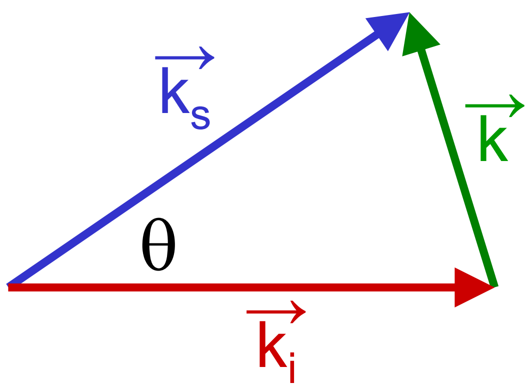

+ gives anti-Stokes interaction
- gives Stokes interaction

Energy conservation:

$$\omega_s = \omega_i \pm \omega$$

Bragg relation follows from high frequency incident wave:

$$\omega_i \gg \omega \Longrightarrow k_i \approx k_s \text{ and}$$

$$k = 2k_i \sin(\theta/2)$$

Fluctuation spectrum can be reconstructed using multiple detection channels

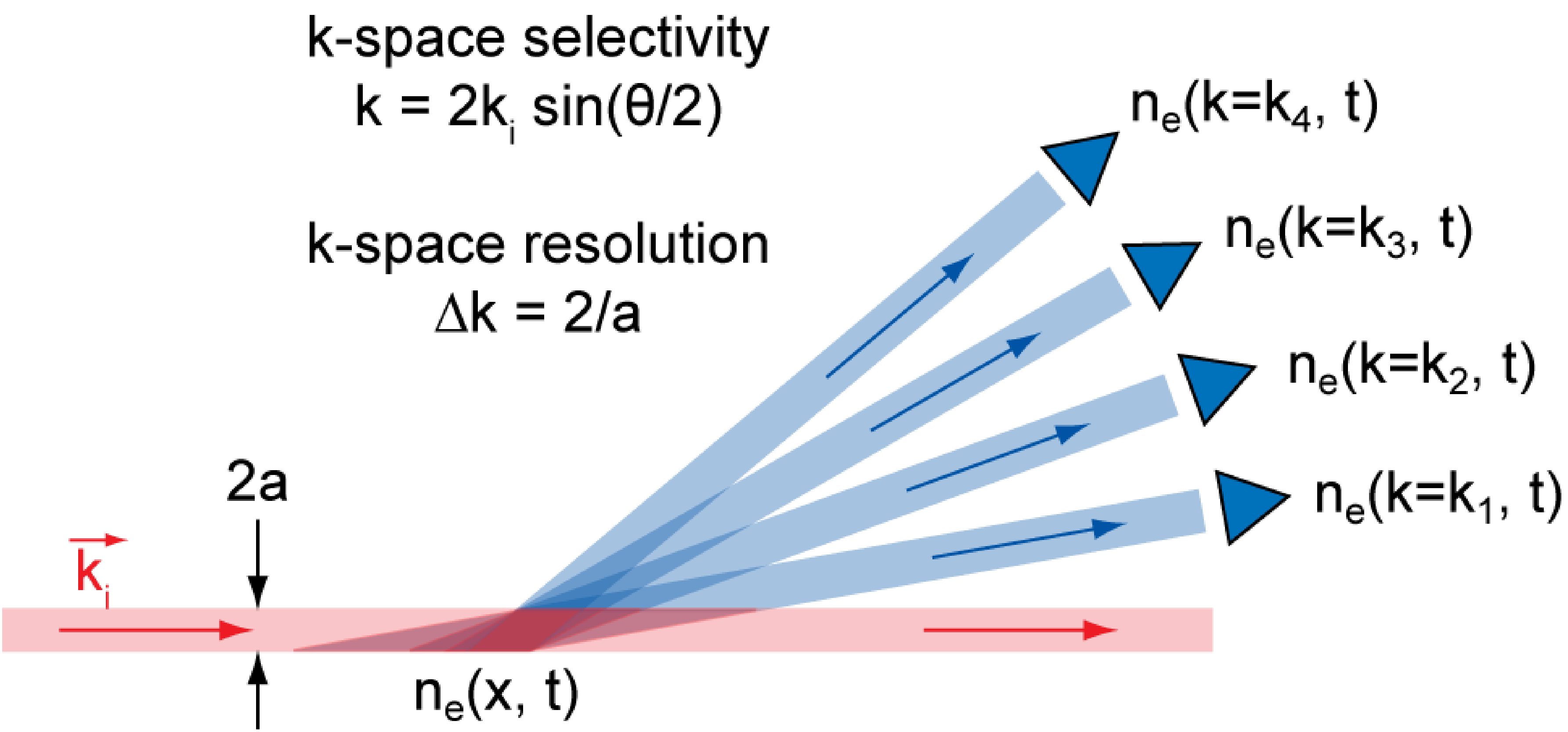

The **plasma** performs the **Fourier transform** from real space to k-space

Anisotropic turbulence and magnetic field variation combine to improve spatial localization

k's and θ's must satisfy:

$$\vec{k} \cdot \vec{B} = 0 \quad \text{and} \quad k = 2k_i \sin(\theta / 2)$$

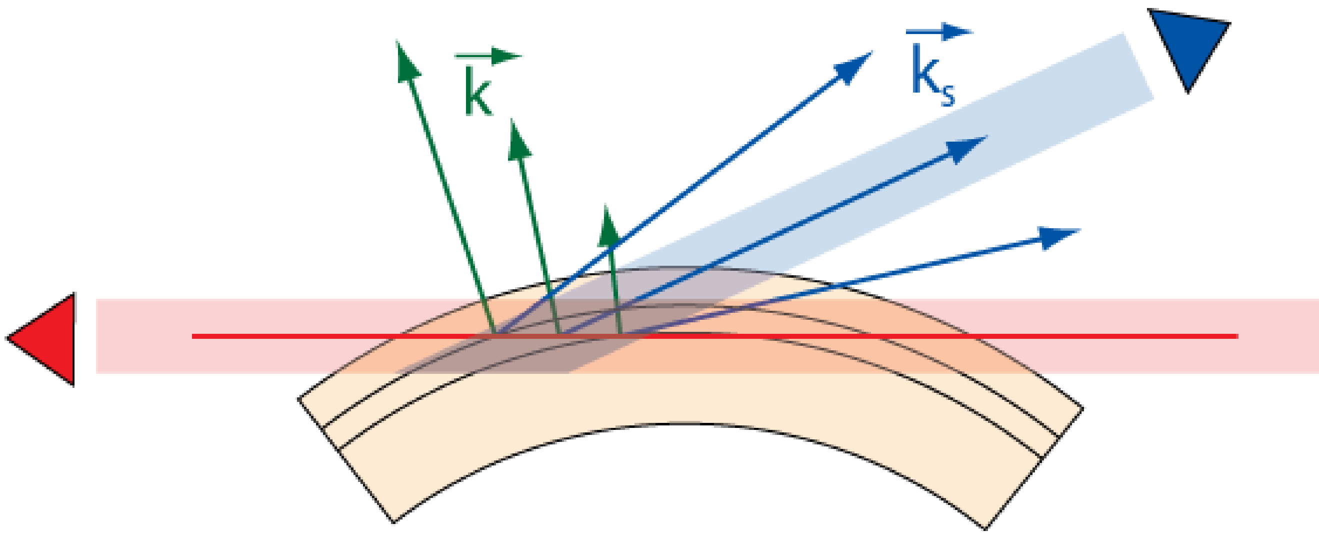

For scattering on the midplane, k's are purely radial.
Some k's within the overlap volume produce scattered light (k_s) that does not intersect the receiver, so the scattering volume is constricted.

see Mazzucato, PPCF 48, 1749 (2006)

Density fluctuations encoded into scattered power spectrum

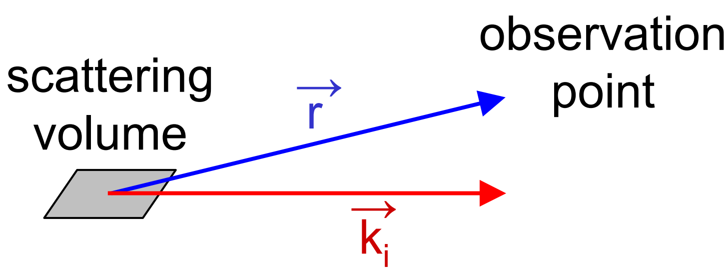

independent quantities:

$$\vec{k}_i \quad \omega_i \quad \vec{r} \quad \omega_s$$

derived quantities:

$$\vec{k}_s \equiv \frac{\omega_s}{c}\hat{r}$$

$$\omega \equiv \omega_s - \omega_i$$

$$\vec{k} \equiv \vec{k}_s - \vec{k}_i$$

$$\frac{d^2 P_s(\vec{r},\omega_s)}{d\Omega\, d\omega_s / 2\pi} = r_e^2 \frac{P_i}{A} \left|\hat{r}\times\hat{r}\times\hat{E}_i\right|^2 \frac{\left|n_e(\vec{k},\omega)\right|^2}{T}$$

Scattered power due to a single, coherent fluctuation:

$$P_s = \frac{1}{4} P_i\, r_e^2\, \lambda_i^2\, \tilde{n}^2\, L_v^2$$

Thomson scattering → EM wave scattering due to unbound electrons

Rayleigh scattering → EM wave scattering due to bound electrons

Scattering cross-section, σ, derives from the dipole radiation of an electron, with natural frequency ω_0, driven by an EM wave with frequency ω:

$$\sigma(\omega) = \frac{\omega^4}{\left(\omega^2 - \omega_0^2\right)^2} r_e^2$$

Thomson scattering

$\omega_0 = 0$

$$\sigma(\omega) = r_e^2$$

Rayleigh scattering

$\omega_0 >> \omega$

$$\sigma(\omega) = \frac{\omega^4}{\omega_0^4} r_e^2 = \frac{\lambda_0^4}{\lambda^4} r_e^2$$

Classical electron radius: $$r_e = \frac{e^2}{4\pi\varepsilon_0 m_e c^2}$$

Two varieties of Thomson scattering: collective and incoherent

- Incoherent Thomson scattering
  - Scattering wavelength → $\lambda \ll \lambda_D$ ($\lambda = 2\pi/k$)
  - Random electron motion → incoherent radiation
  - Dipole powers additive → $P_s \propto n_e$
  - Near-IR sources → $\lambda \sim 1\ \mu m$
  - Scattering angle → 90°
  - Useful for n_e and T_e measurements
- Collective Thomson scattering
  - Scattering wavelength → $\lambda \gtrsim \lambda_D$
  - Collective electron motion → coherent radiation
  - Dipole powers multiplicative → $P_s \propto n_e^2$
  - Far-IR to mm-wave sources → $\lambda \sim 10\ \mu m$ to 4 mm
  - Scattering angles → 1° to 40°
  - Useful for density fluctuation measurements

The NSTX high-k scattering system

NSTX "high-k" scattering system measures fluctuations up to $k_\perp \rho_e \cong 0.6$

- 280 GHz (λ=1 mm) scattering system
- Instrumental minimum detectable fluctuation is $\tilde{n}_e/n_e \sim 10^{-5}$
- Five detection channels
  - $k_\perp$ spectrum at five discrete $k_\perp$
  - ω spectrum from time domain sampling
- Tangential scattering
  - Probe and receiving beams nearly on equatorial midplane
  - System sensitive to radial fluctuations
- Steerable optics
  - Scattering volume can be positioned throughout the outer half-plasma
- First data during FY06 run campaign

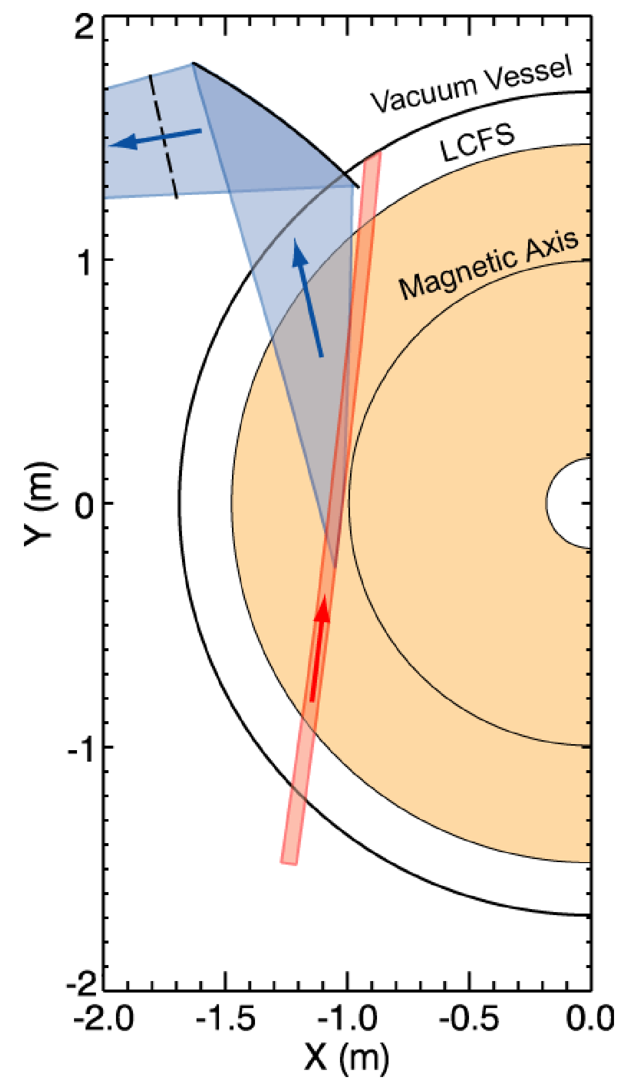

Five detection channels can measure fluctuations at five discrete wavenumbers

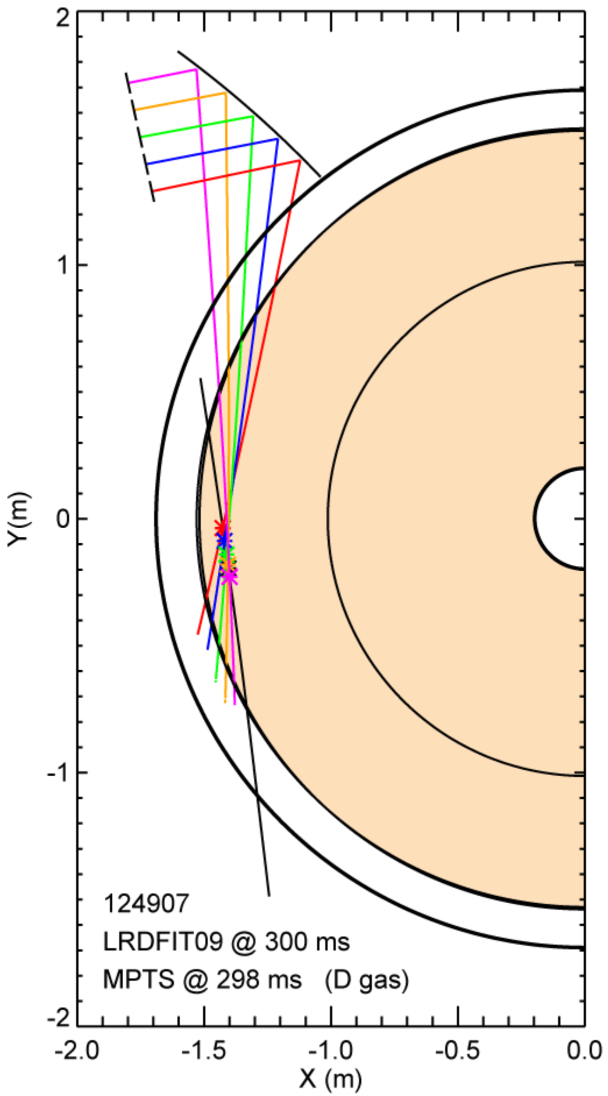

Measurements at

R = 142 cm and r/a = 0.79

higher k, smaller λ ⟷ lower k, larger λ

	Ch. 1	Ch. 2	Ch. 3	Ch. 4	Ch. 5
$k_\perp$ (cm^{-1})	21.4	17.1	12.8	9.0	5.3
$k_\perp \rho_e$	0.31	0.25	0.19	0.13	0.08
$k_\perp \rho_s$	18.9	15.2	11.6	8.2	4.8
$\lvert k_\theta / k_r \rvert$	0.19	0.18	0.18	0.17	0.17

Steerable optics enable good radial coverage

Inboard $\rho = 0.05$
$k_{\perp}\rho_e$ up to 0.7

Intermediate $\rho = 0.4$
$k_{\perp}\rho_e$ up to 0.3

Outboard $\rho = 0.75$
$k_{\perp}\rho_e$ up to 0.2

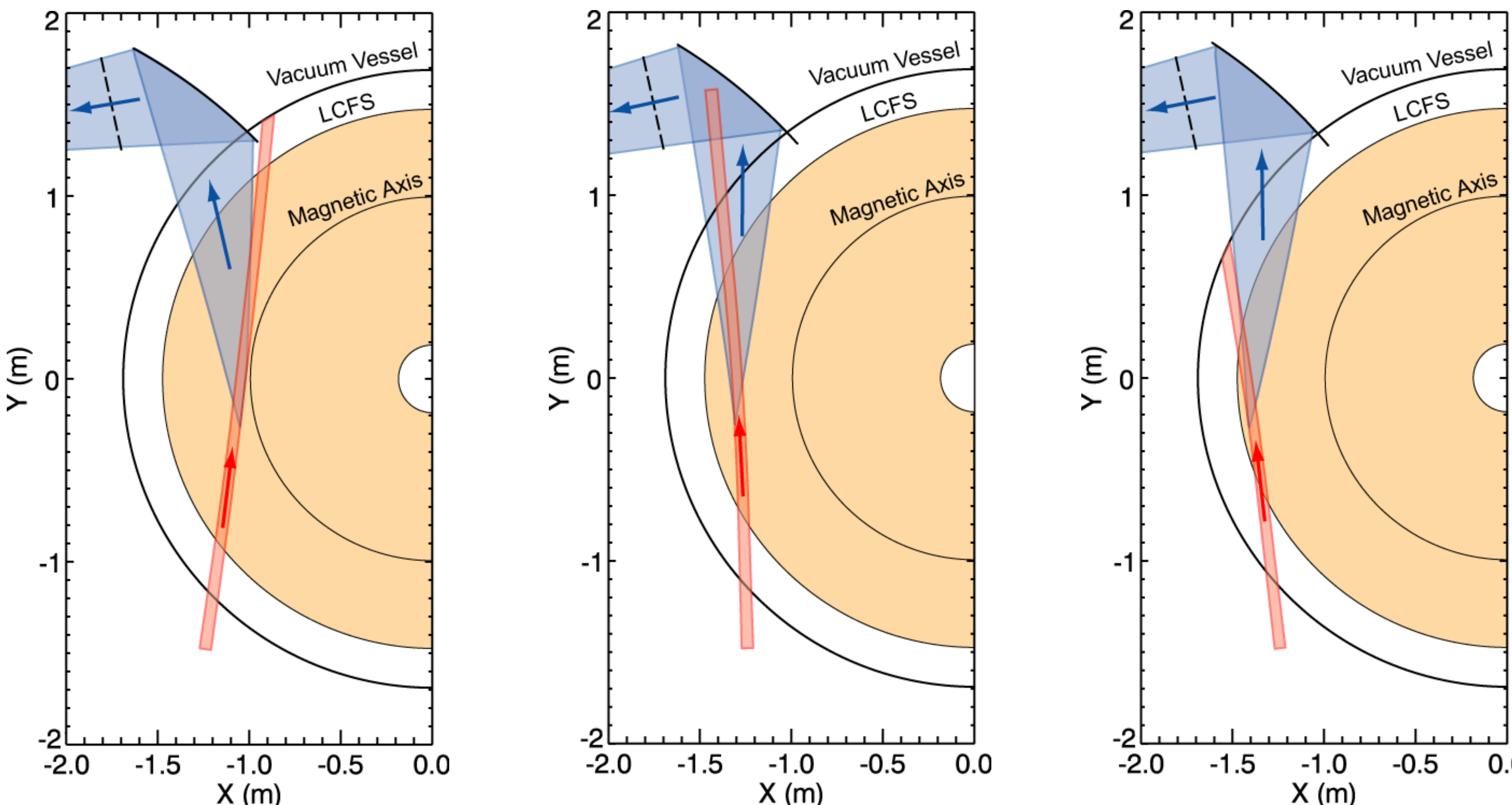

Scattering system layout

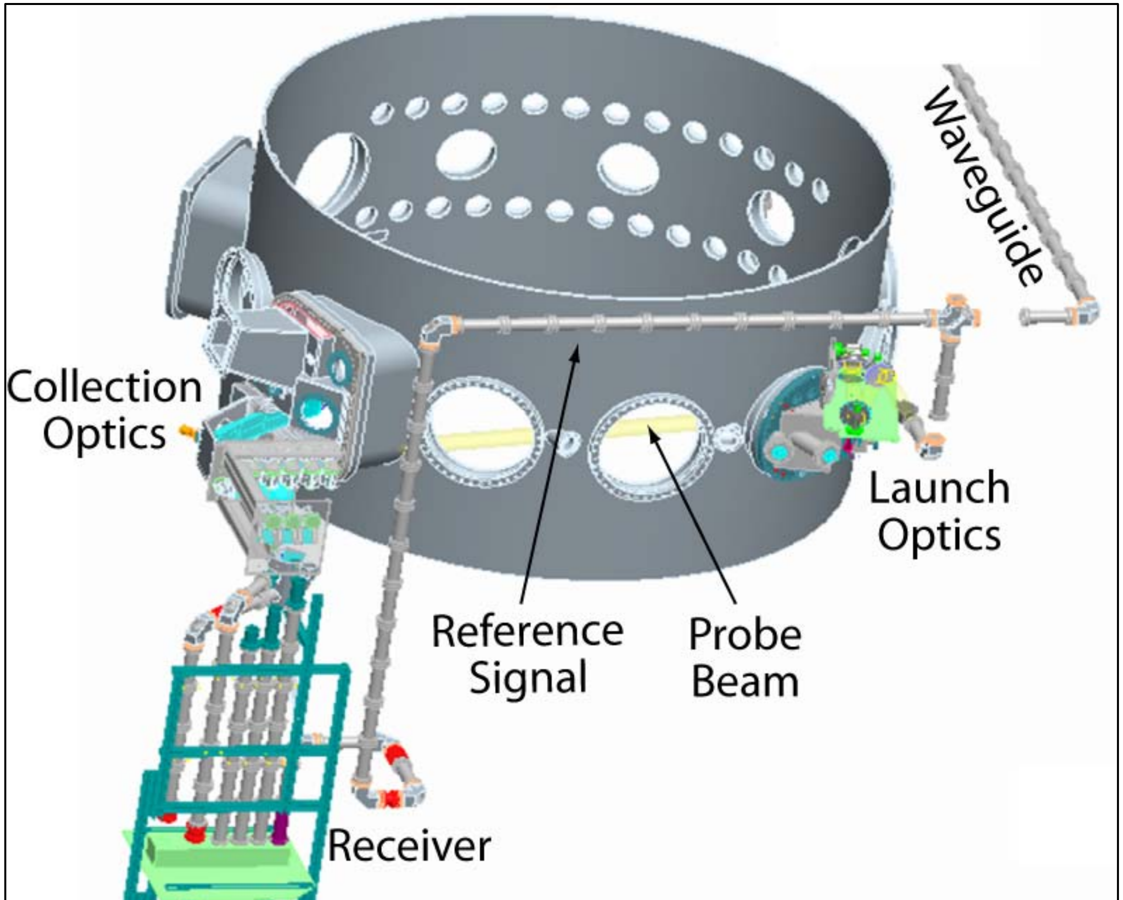

- BWO source
  - outside test cell
  - ~100 mW at 280 GHz
- Overmoded, corrugated waveguide
  - low-loss transmission
- Steerable optics
  - quasi-optical design
- Heterodyne receiver
  - five channels
  - reference signal extracted from main beam

Scattering system pictures

waveguide and launch optics

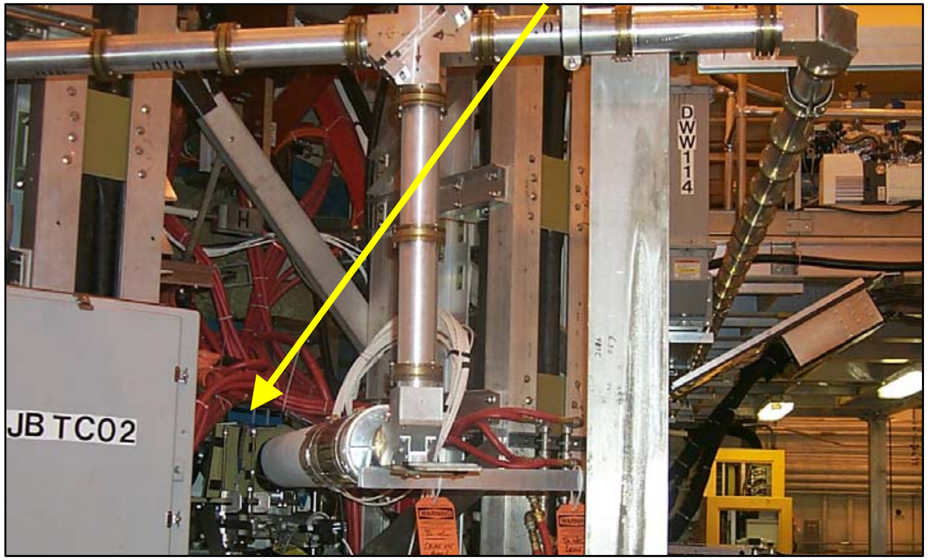

collection optics

exit windows

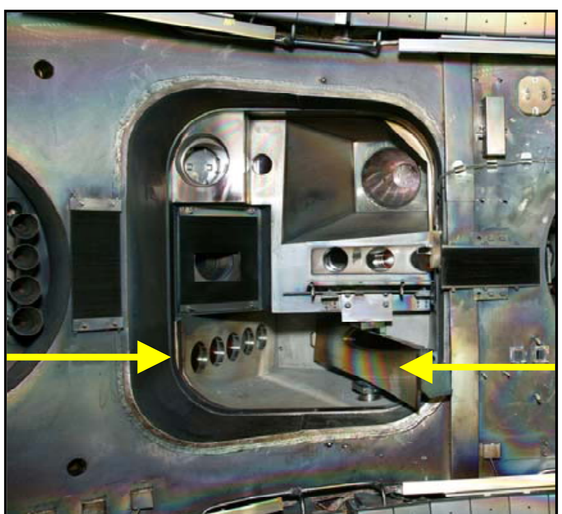

collection mirror

heterodyne receiver

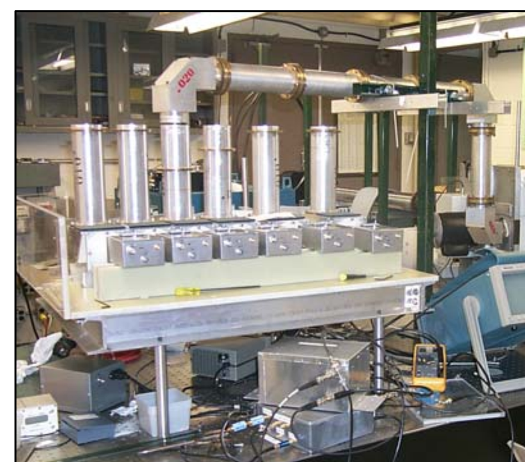

Quasi-optical design positions beam waist at scattering location and couples scattered light into receiver

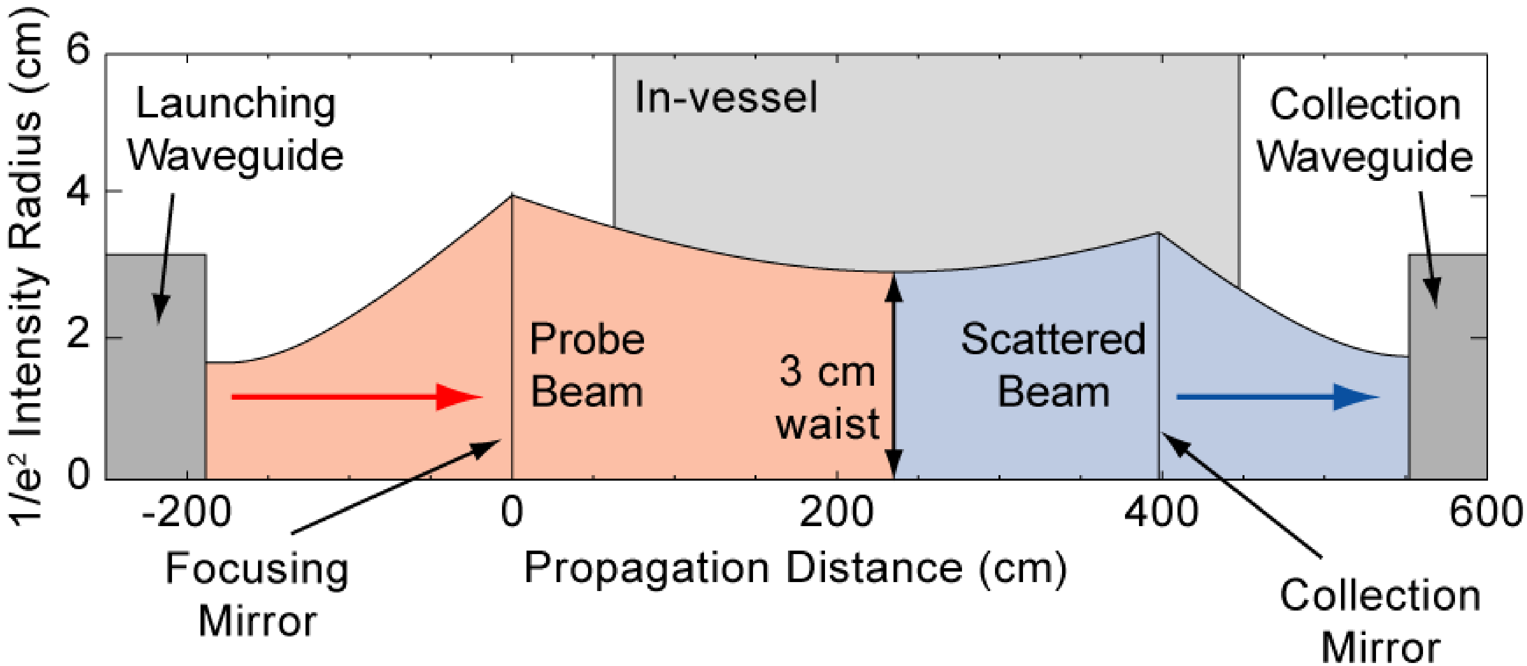

- 3 cm beam waist (1/e^2 intensity radius) at the scattering location
- k-space resolution $\Longrightarrow$ $\Delta k \approx 0.7$ cm^{-1}

Quadrature heterodyne receiver samples at 7.5 MS/s

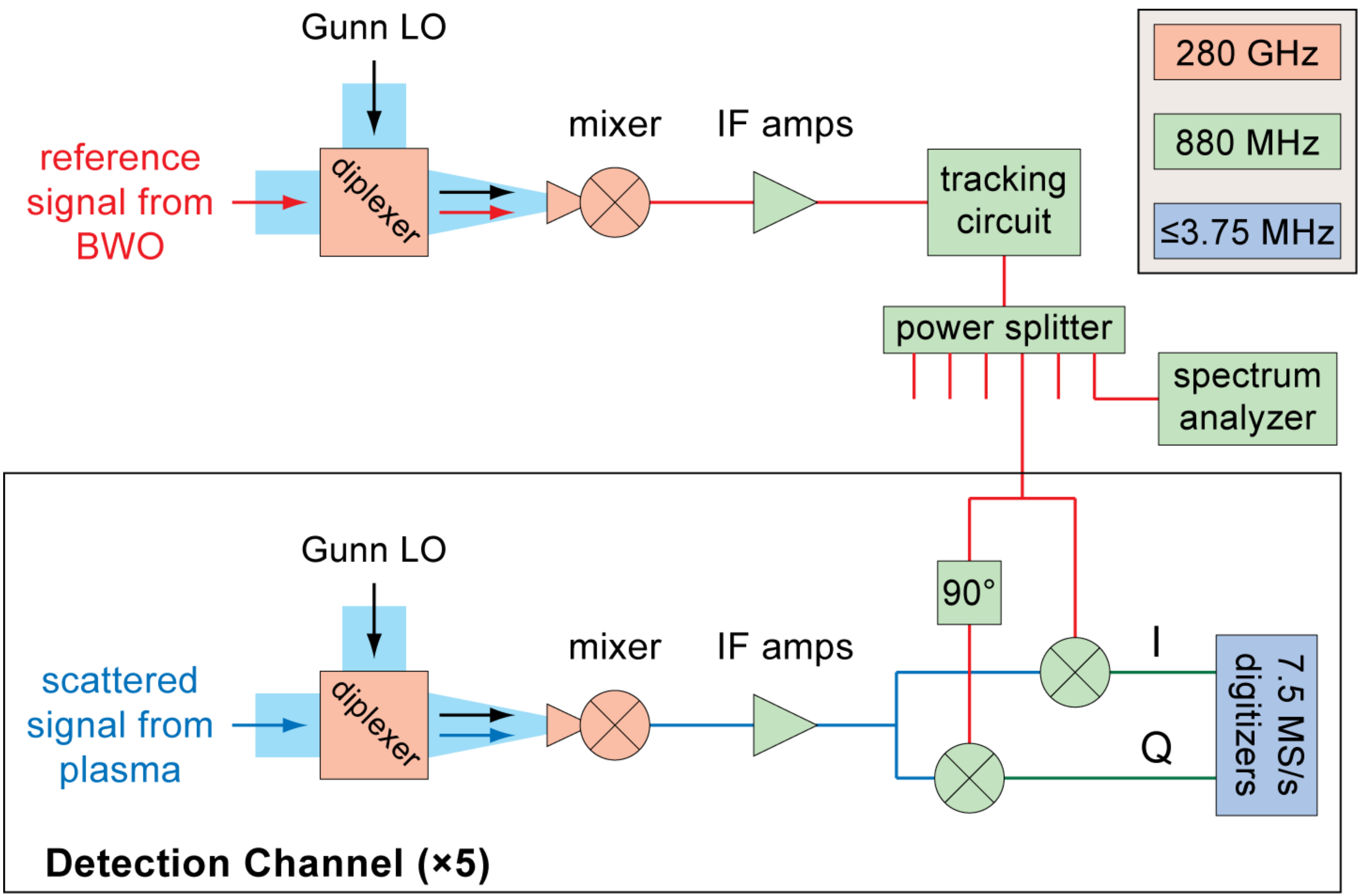

Ray tracing calculations are needed to design configurations prior to experiments

NSTX

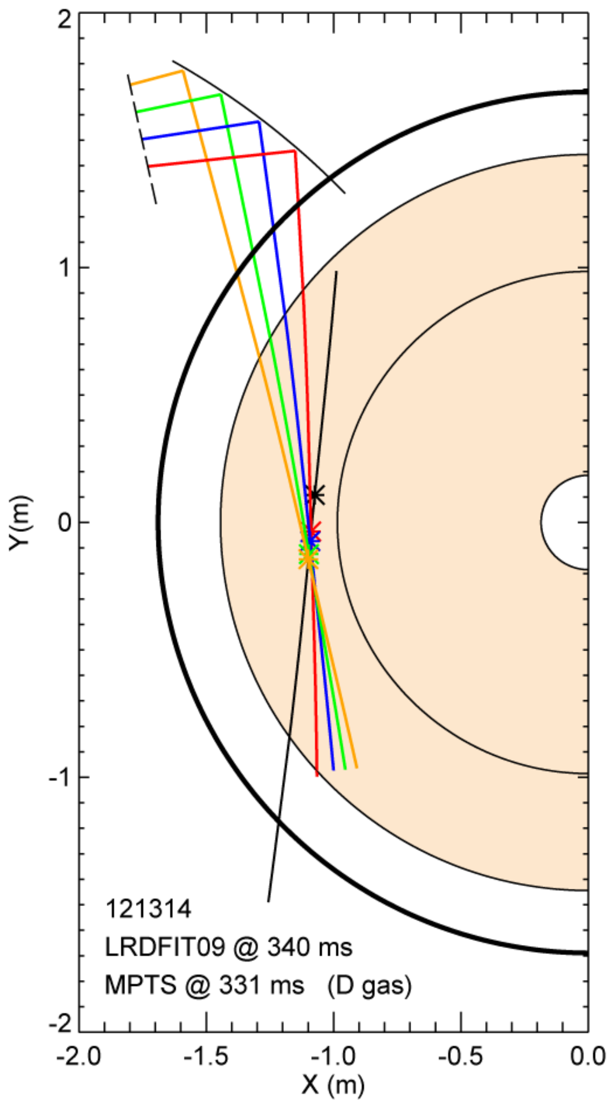

Launch mirror (probe beam)

Horizontal actuator: 1.117 in.

Horizontal angle wrt X-axis: 83.0°

Vertical actuator: 1.217 in.

Vertical angle wrt midplane: -6.0°

Collection mirror

Horizontal actuator: 2.144 in.

Horizontal angle wrt X-axis: 232.5°

Vertical angle wrt midplane: 5.4°

(Vertical angle not adjustable)

Exit window angles				
	Ch. 2	Ch. 3	Ch. 4	Ch. 5
Hor. Ang.	-6.4°	-3.9°	-0.7°	2.5°
Vert. Ang.	-0.2°	-0.7°	-1.1°	-1.5°

Ray tracing calculations are needed to ensure k-space alignment

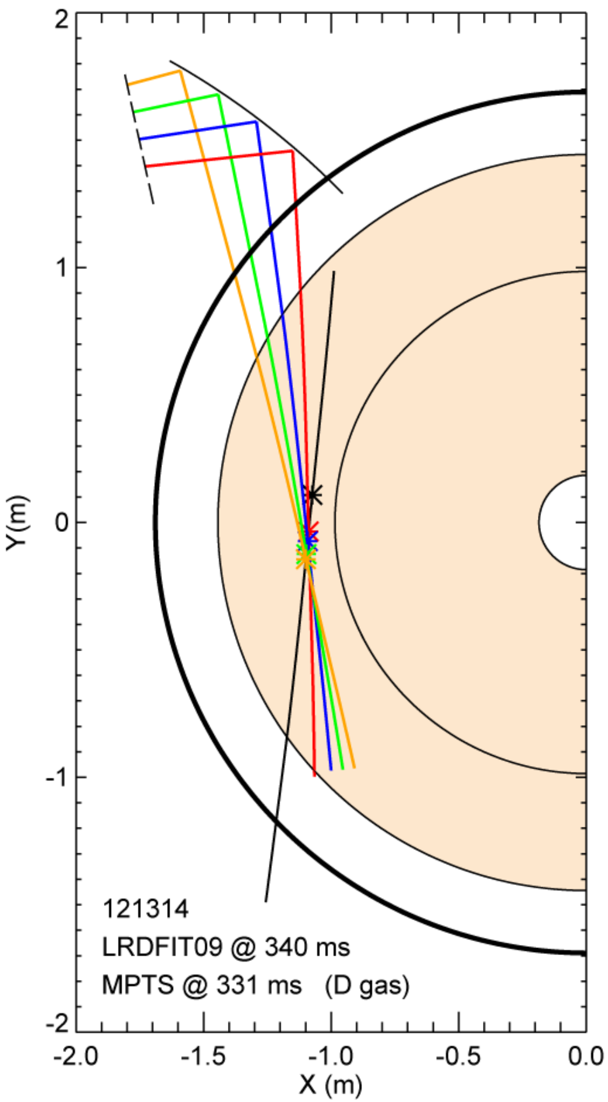

	Ch. 2	Ch. 3	Ch. 4	Ch. 5
r/a	0.27	0.28	0.29	0.30
d_{min} (cm)	0.1	0.1	0.1	0.1
$k_{\parallel}$ (cm^{-1})	0.1	0.0	0.2	0.0
k_r (cm^{-1})	6.9	11.0	14.6	17.8
k_θ (cm^{-1})	-1.6	-3.4	-4.4	-5.5
$k_\perp$ (cm^{-1})	7.1	11.5	15.2	18.6
$\lvert k_\theta/k_r \rvert$	0.23	0.30	0.30	0.31
$k_\perp \rho_e$	0.23	0.38	0.51	0.62
$k_\perp \rho_s$	14	22	30	37
k_T (cm^{-1})	-0.4	-0.7	-1.2	-1.3
f_D (MHz)	-0.95	-1.78	-2.98	-3.26
d_{tan} (cm)	-14.5	-18.4	-23.5	-25.5

Data is not junk

Electron diamag. direction

Doppler shift in ion direction

Offset from PB tangency

Ray tracing calculations are needed to determine scattering volume size

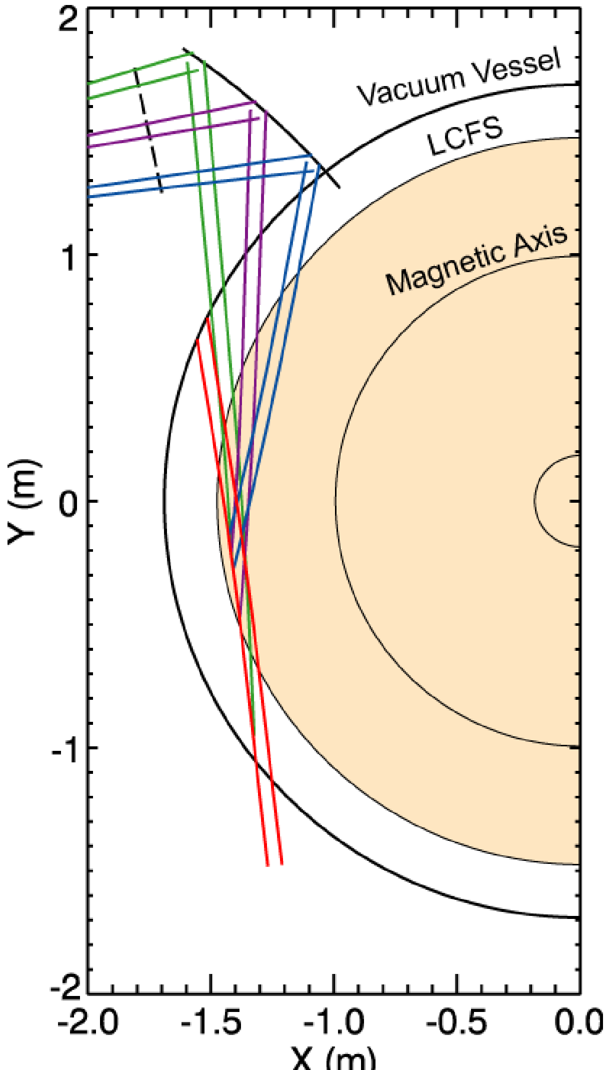

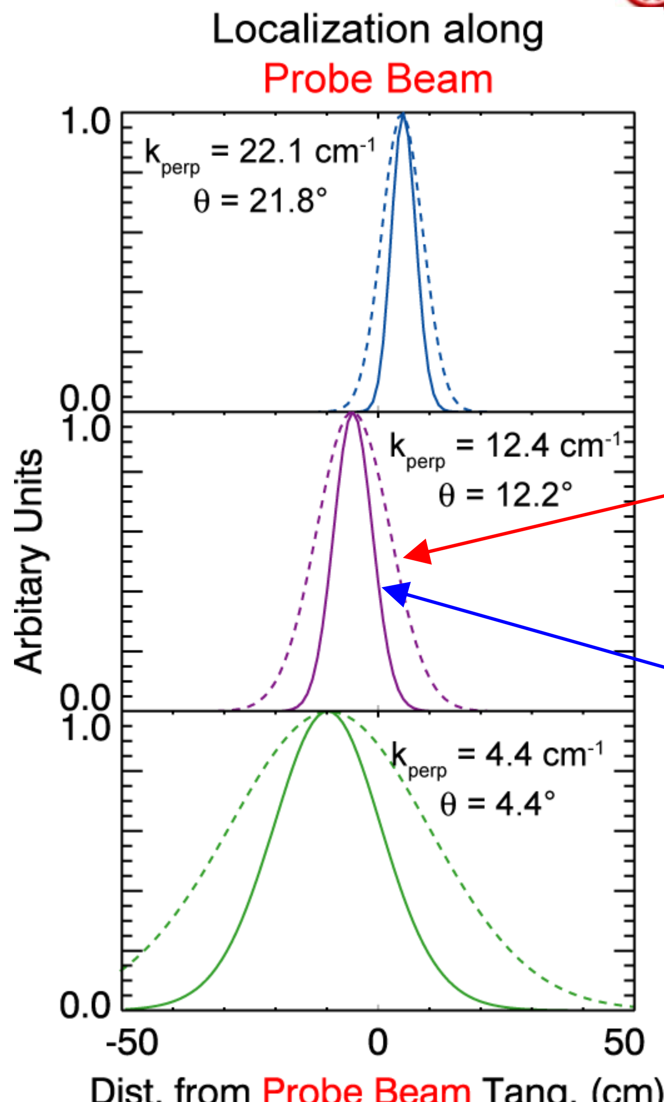

beam overlap

instrument selectivity due to $k_\perp \gg k_\parallel$

Ray tracing calculations are needed to account for refraction

with refraction

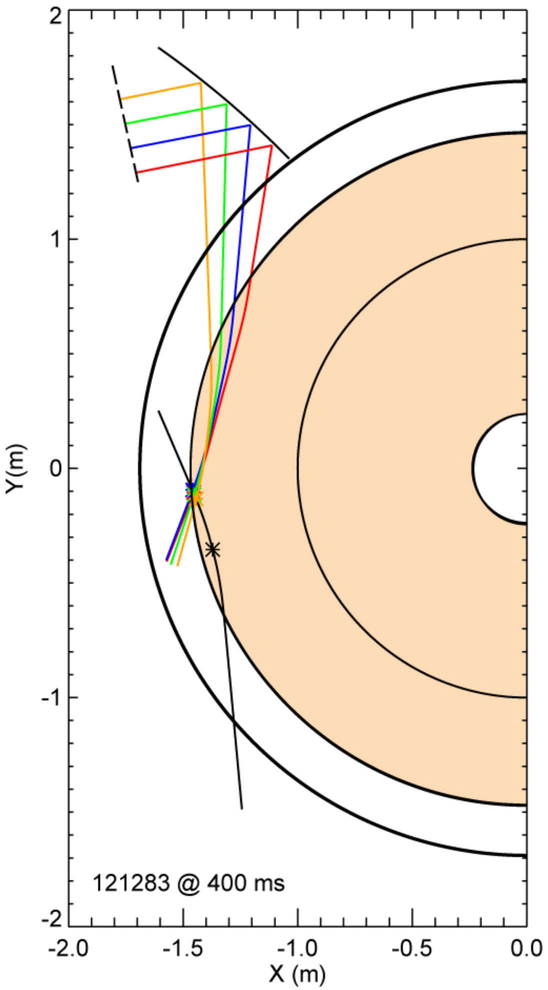

without refraction

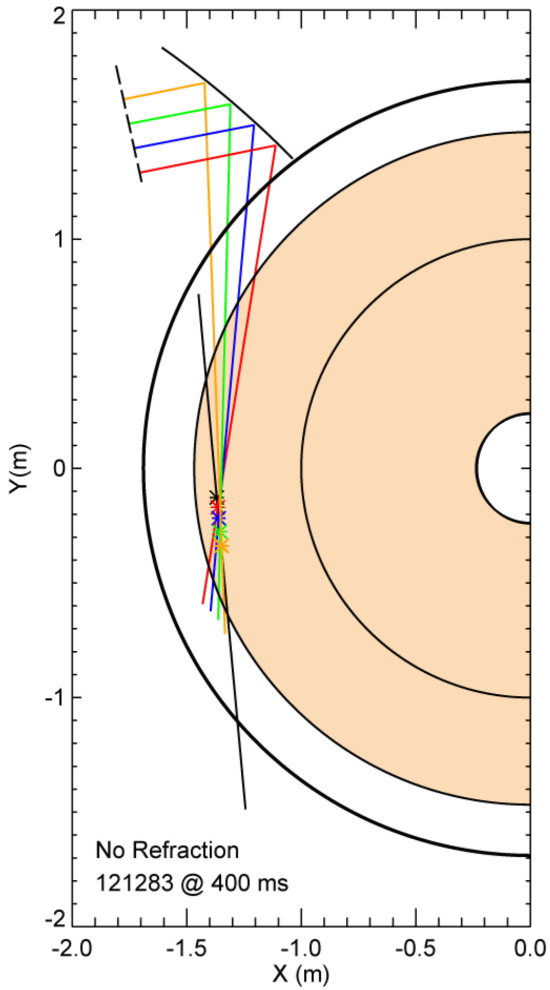

	Ch. 1	Ch. 2	Ch. 3	Ch. 4
with refraction				
r/a	0.99	1.00	0.99	0.97
$k_\perp$	44.1	43.8	41.2	37.4
without refraction				
r/a	0.81	0.82	0.82	0.84
$k_\perp$	14.8	10.7	6.9	3.3

Ray tracing calculations are needed to discriminate good data from junk data

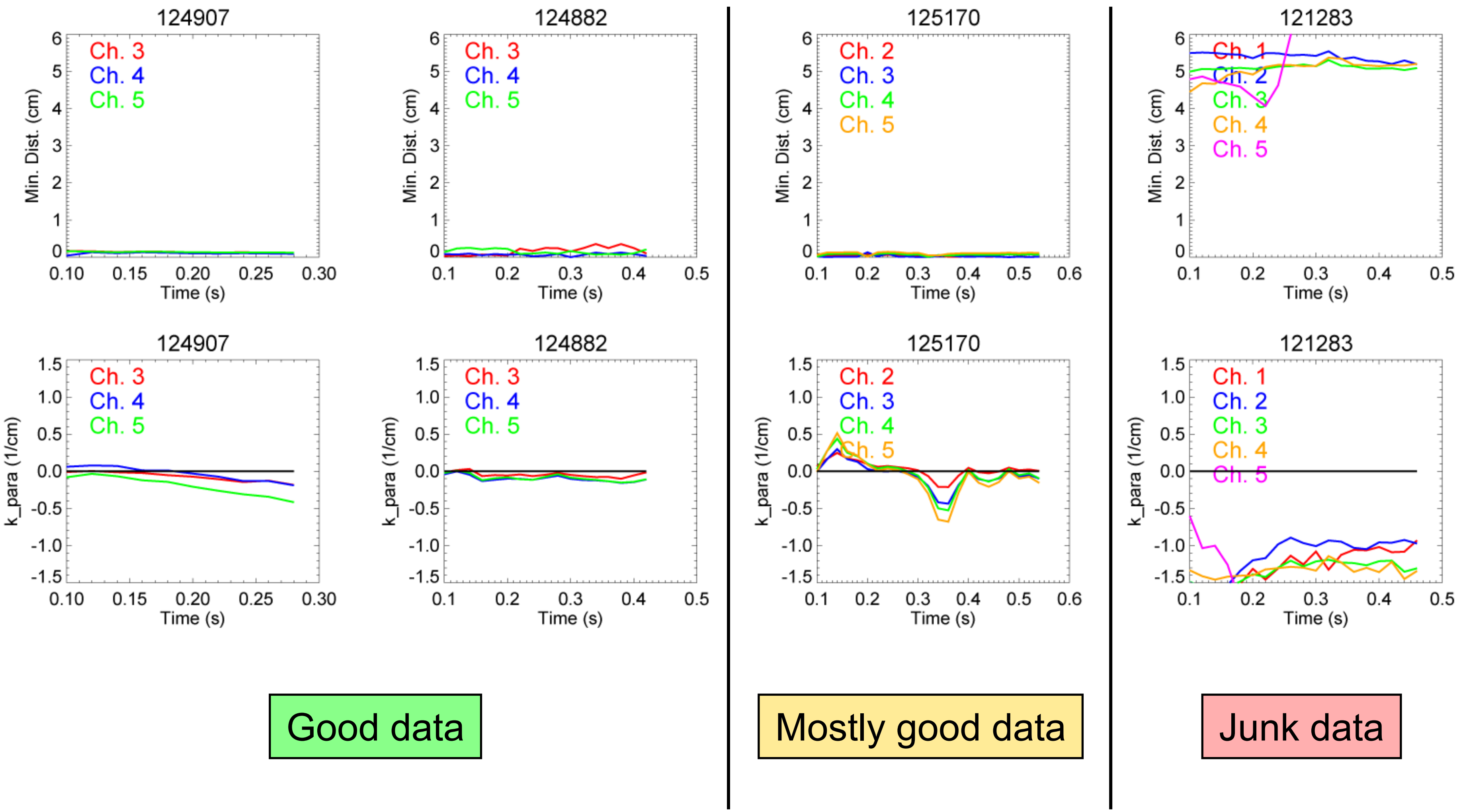

Good data

Mostly good data

Junk data

Ray tracing calculations are needed to interpret measurements

The time evolution of turbulence parameters, such as $k_{\perp}\rho_e$ and k_{θ}/k_r, are needed for comparing data to simulations.

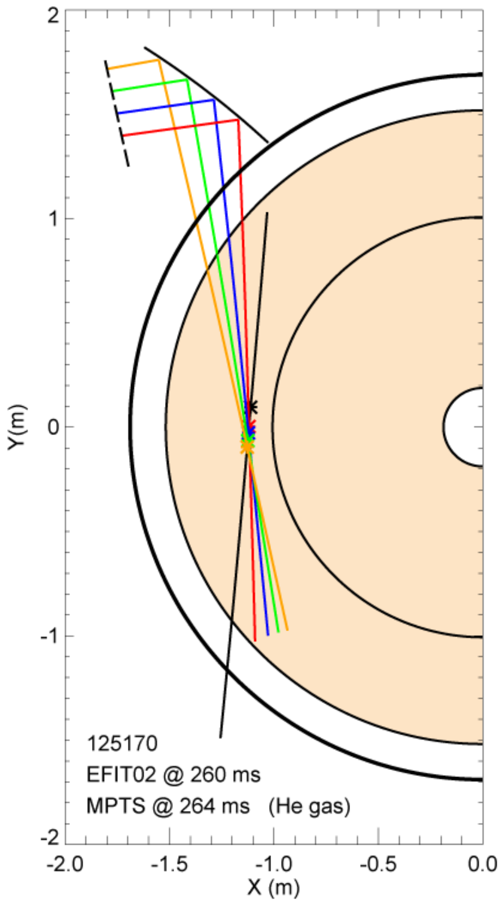

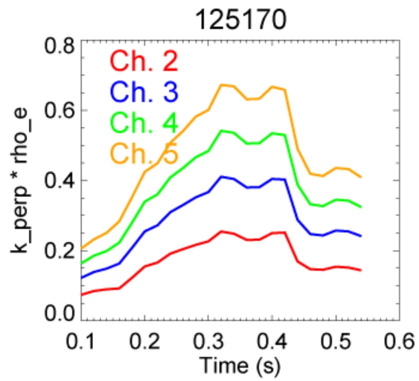

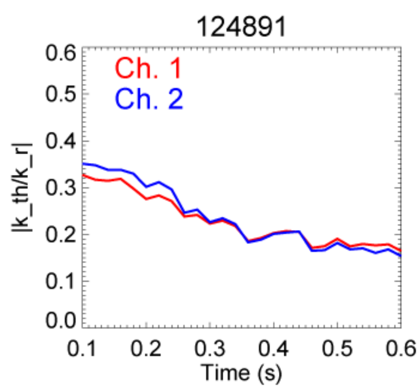

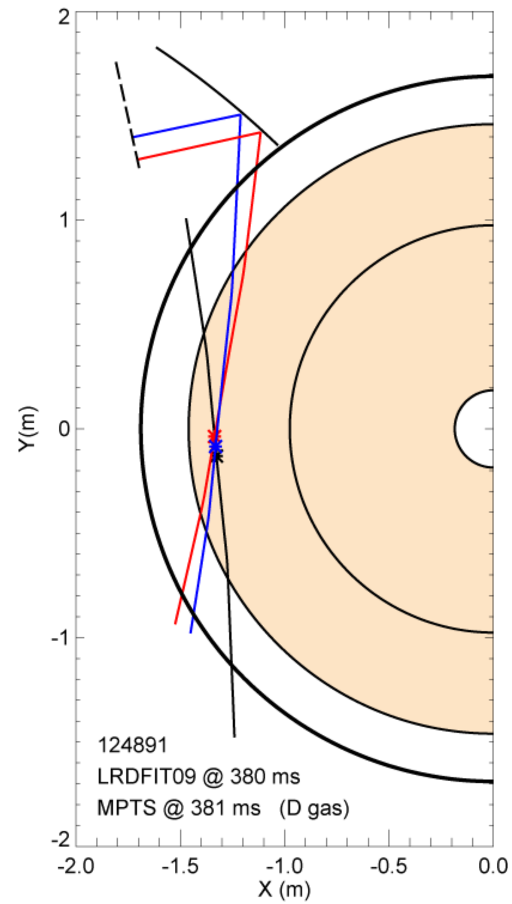

Initial measurements and research topics

Stray light spectral peak and Doppler-shifted fluctuations are common features

High-k measurements at R ≅ 135 cm and r/a ≅ 0.68 with $k_\perp \rho_e$ ~ 0.2-0.3

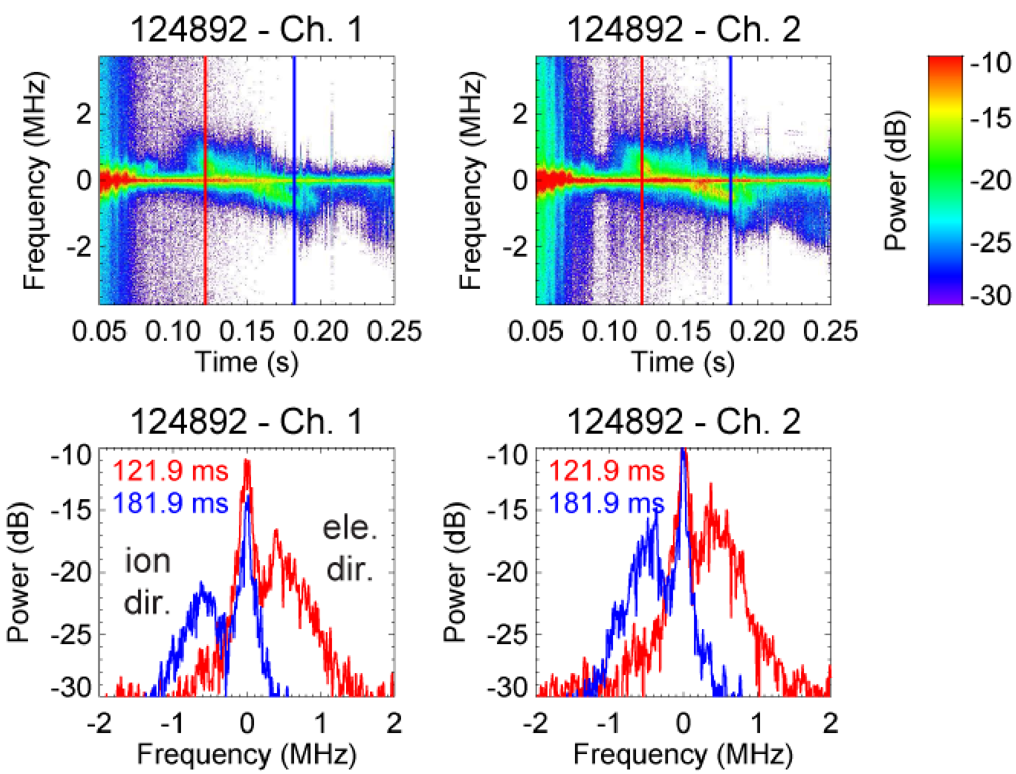

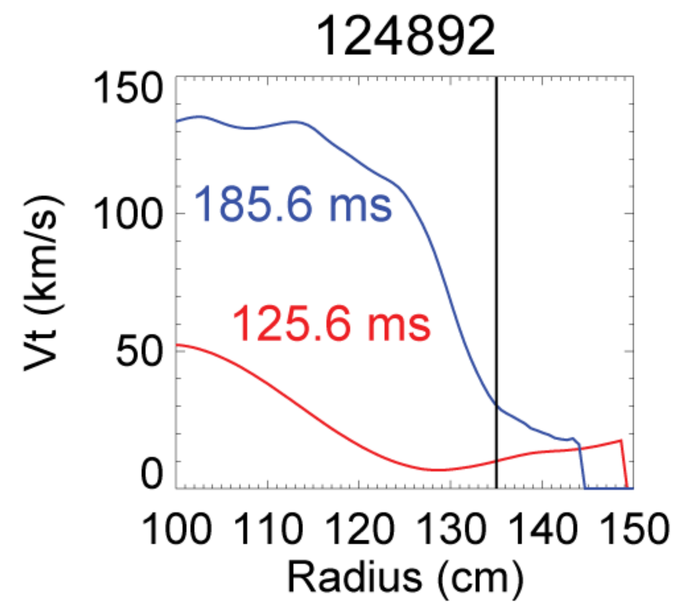

Fluctuations initially appear in the **electron direction,** then Doppler-shift to the **ion direction** due to V_T**.**

Prominent, persistent fluctuations observed in core

High-k measurements at R ≅ 113 cm and r/a ≅ 0.25

$k_{\perp}\rho_e$ ~ 0.35-0.40 for channel 5

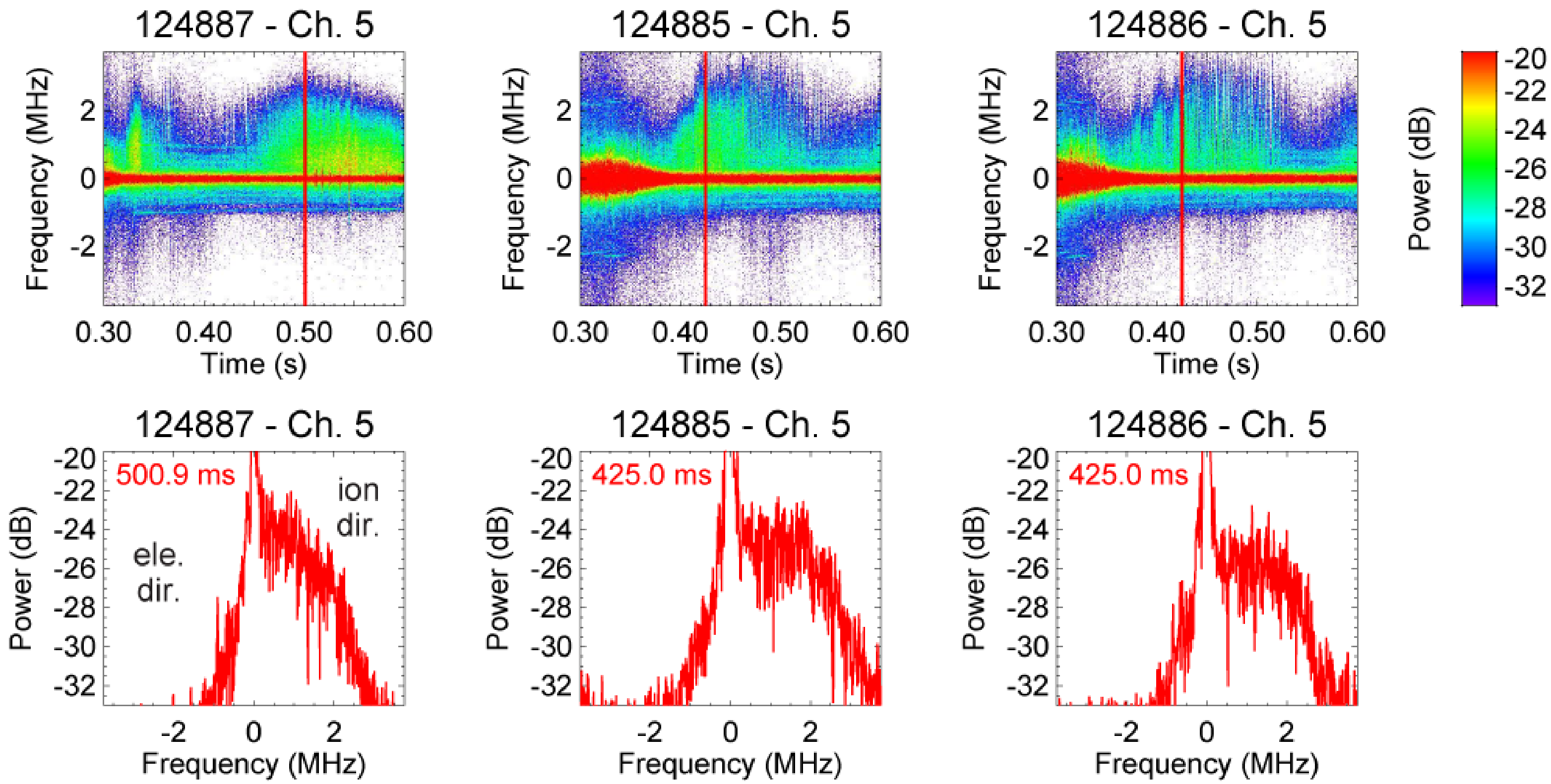

Features appear in the ion direction due to Doppler shift

Core fluctuations grow when R/L_{Te} is near critical value

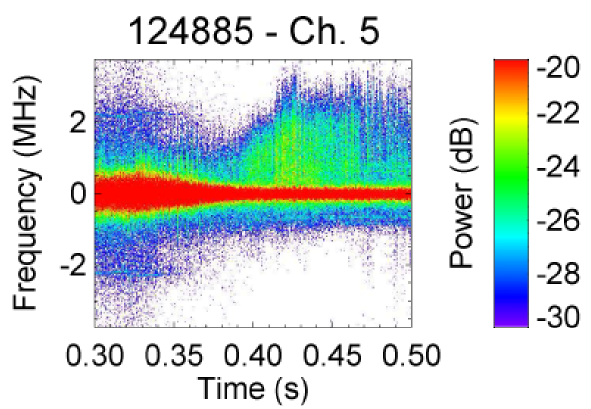

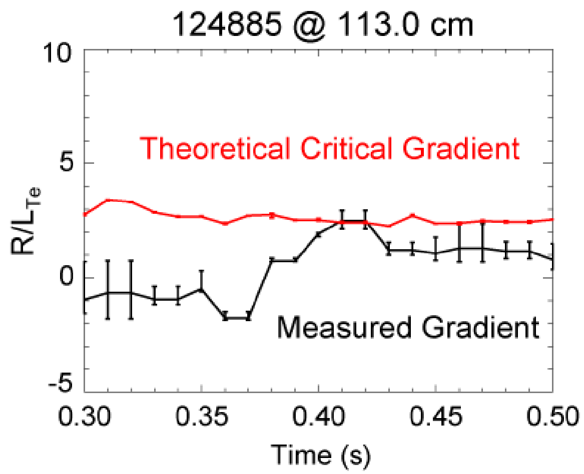

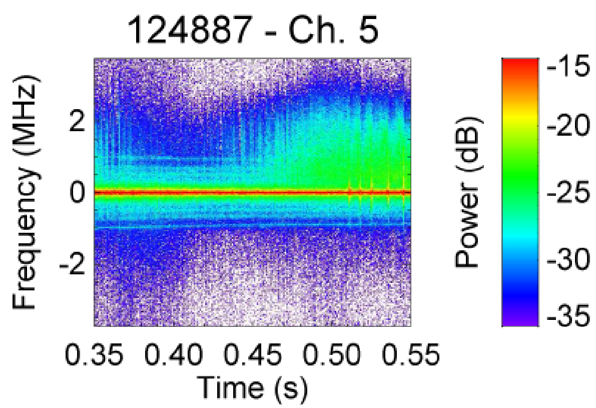

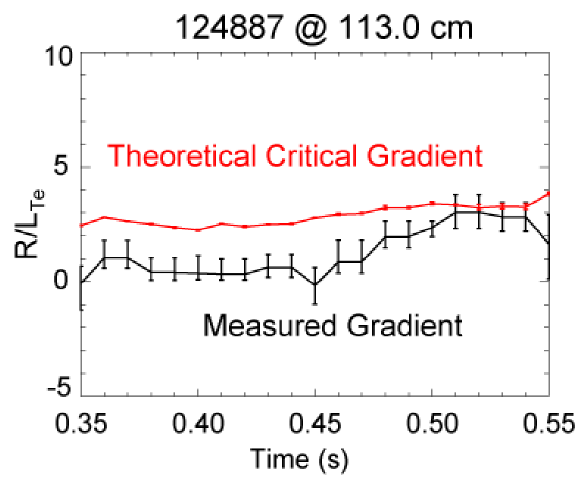

Prominent, persistent fluctuations observed in outer-plasma

High-k measurements at R ≅ 135 cm and r/a ≅ 0.7

$k_\perp \rho_e \sim 0.1\text{-}0.3$ for channel 2

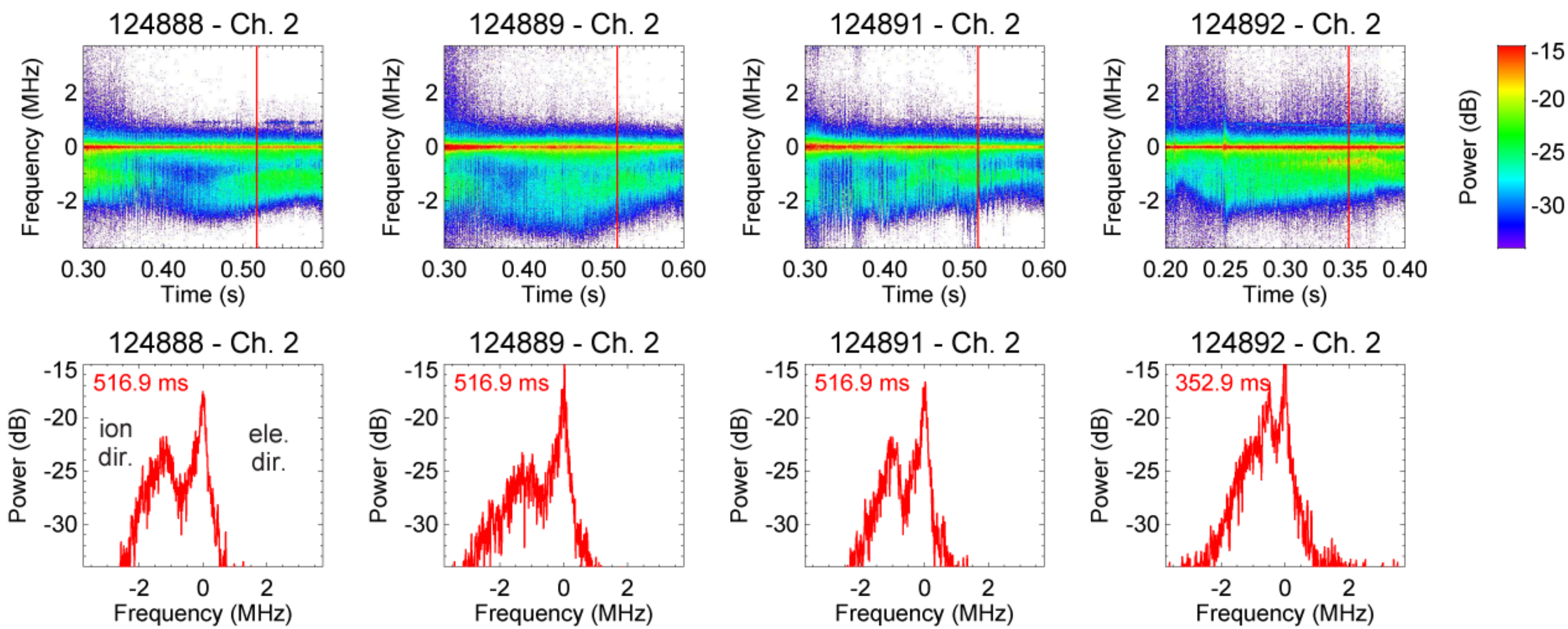

Ion/electron directions are reversed from previous slide.
Fluctuations again experience a Doppler-shift to ion direction.

Using only HHFW heating, unshifted fluctuations observed in core

High-k measurements at R ≅ 120 cm and r/a ≅ 0.3

$k_\perp \rho_e \sim 0.15\text{-}0.35$ for channel 4

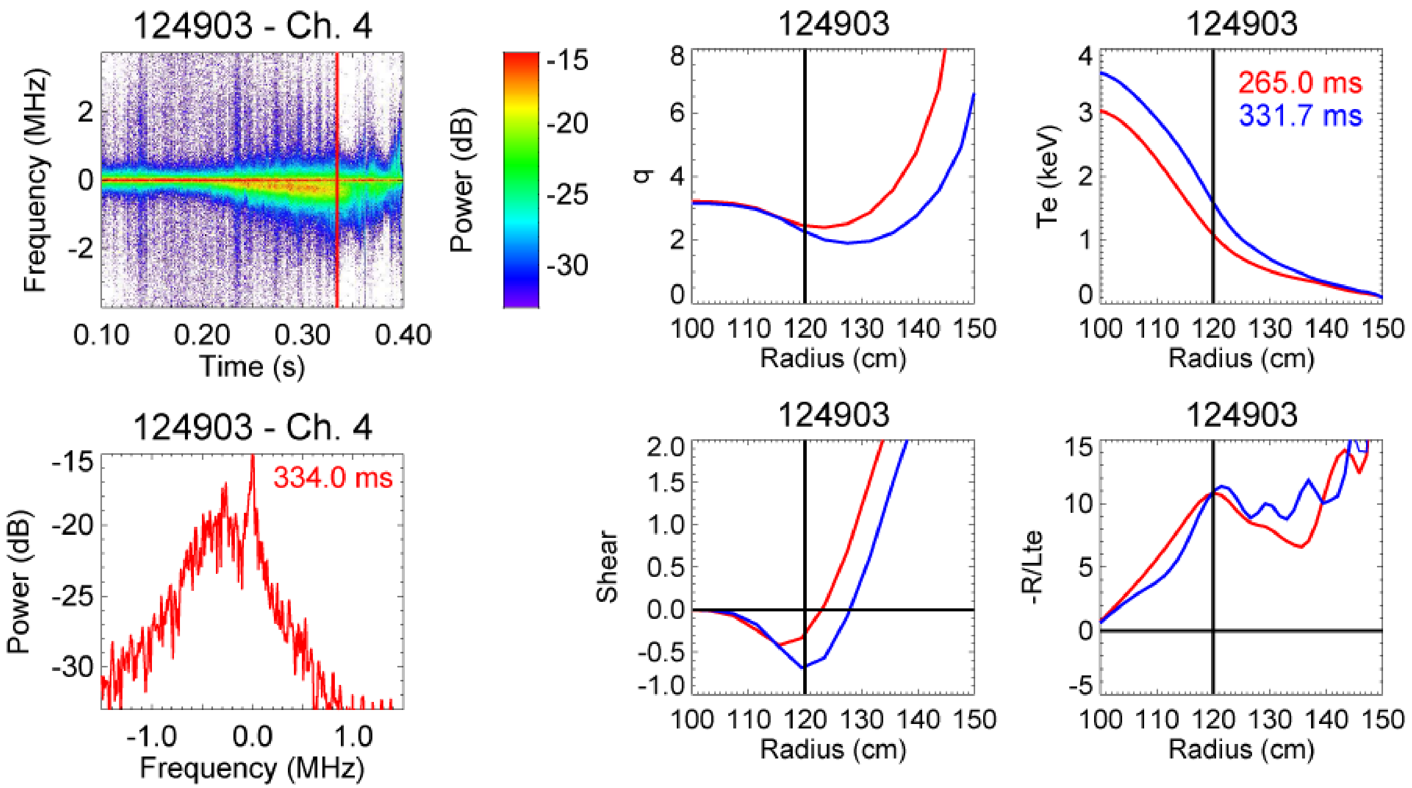

Without toroidal rotation from NBI to produce a Doppler-shift to the ion direction, fluctuations appear in electron direction.

In some HHFW discharges, peak T_e obtained when R/L_n reverses and fluctuations drop

High-k measurements at R ≅ 120 cm and r/a ≅ 0.3

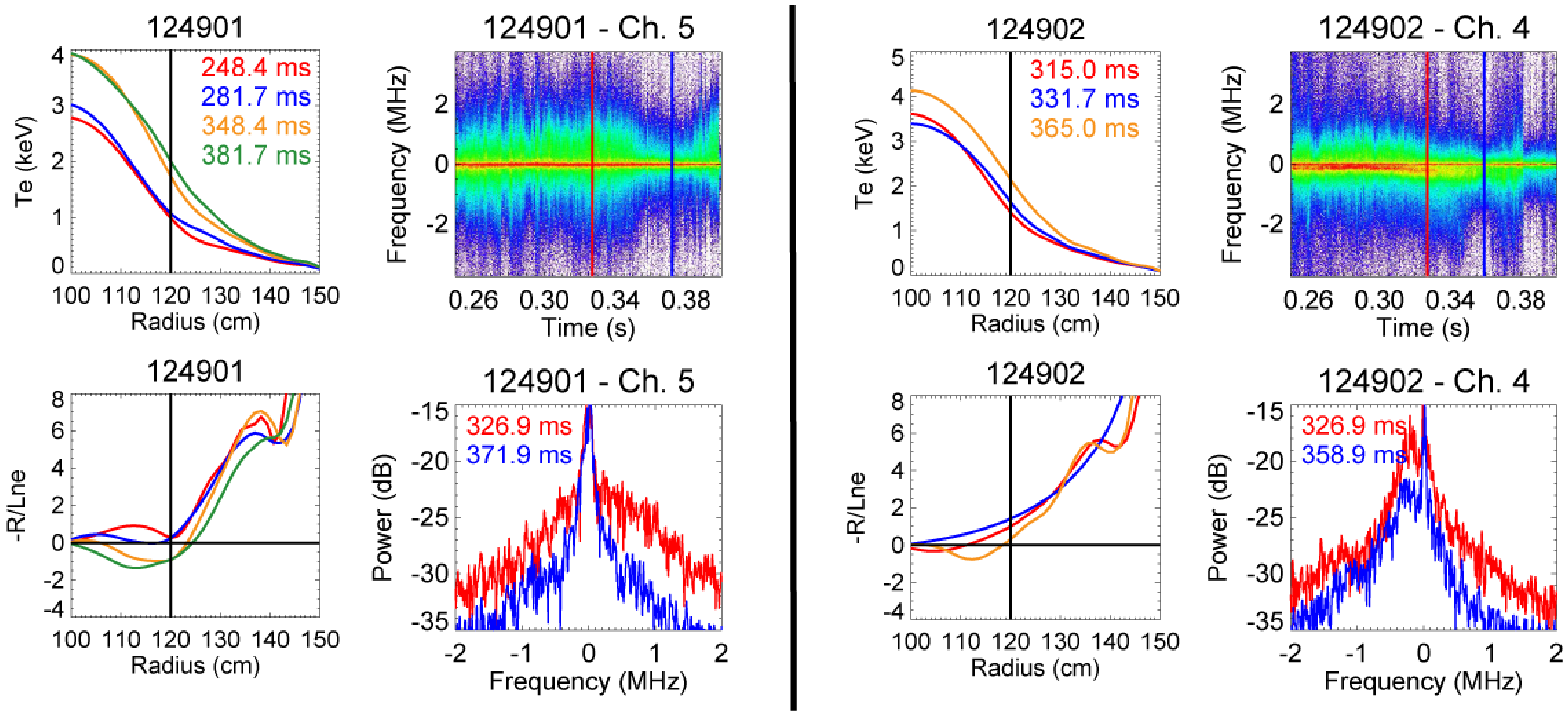

This is a preliminary observation; counter examples exist.

Core fluctuations change character after RS collapse

High-k measurements at R ≅ 120 cm and r/a ≅ 0.35

$k_\perp \rho_e$ ~ 0.15-0.25 for channel 4 and 0.25-0.35 for channel 5

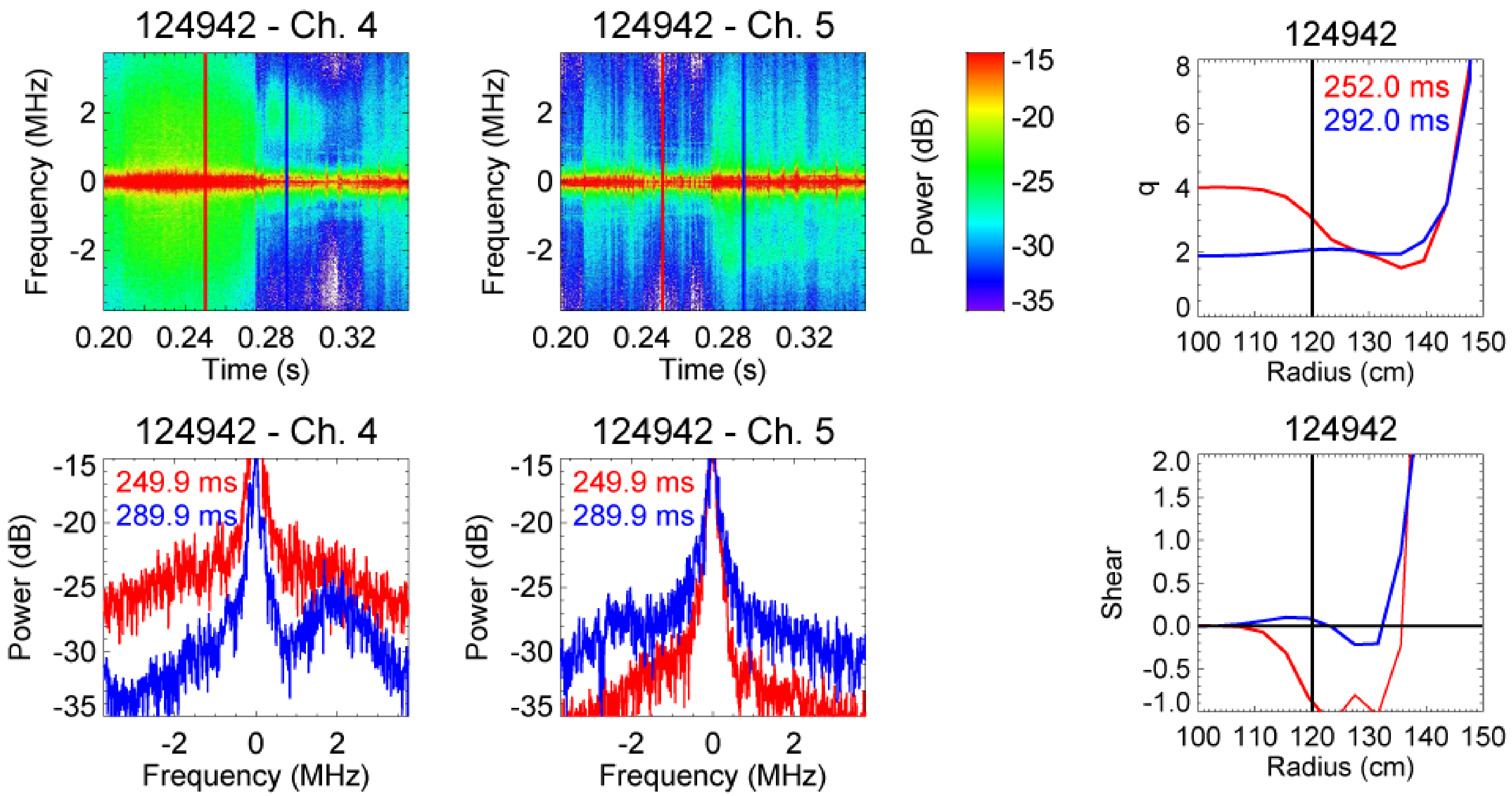

This is a preliminary observation due to stray light concerns.

Unique capabilities may guide future research

The NSTX high-k system is the only core fluctuation diagnostic capable of addressing these questions:

k-space isotropy

– Are fluctuations isotropic in the k_θ-k_r plane?
– Steerable optics provide the capability to address this.

Mode coupling

– What is the phase coherence among three turbulent fluctuations that satisfy frequency and wave vector matching conditions?
– Multiple detection channels provide the capability to address this.

Summary

- Transport is important
- ETG turbulence may be important
- Collective scattering is a powerful technique for measuring fluctuations with spatial localization and k-space selectivity
- The NSTX high-k system is versatile due to steerable optics and multiple detection channels
- Electron gyro-scale fluctuations have been observed exhibiting a variety of dynamics in a variety of NSTX plasmas

Acknowledgements

Special thanks to Ben LeBlanc, Ron Bell, Mike Bell, Russ Feder, Stan Kaye, Howard Yuh, Fred Levinton, Joel Hosea, Dave Mikkelson, Greg Hammett, and T.S. Hahm.